

# Aircraft ice-nucleating particle and aerosol composition measurements in the Western North American Arctic

Alberto Sanchez-Marroquin<sup>1</sup>, Sarah L. Barr<sup>1</sup>, Ian T. Burke<sup>1</sup>, James B. McQuaid<sup>1</sup>, Benjamin J. Murray<sup>1</sup> (\*)

<sup>1</sup>School of Earth and Environment, University of Leeds, Woodhouse Lane, Leeds, LS2 9JT, UK

(\*) Corresponding author: b.j.murray@leeds.ac.uk

Knowledge of the temperature dependent concentration of ice-nucleating particles (INPs) is crucial to understanding the properties of mixed-phase clouds. However, the sources, transport and removal of INPs around the globe, and particularly in the Arctic region, are poorly understood. In the Arctic winter and spring, when many local sources are covered by ice and snow, it is not clear which INP types are important. In this study, we present a new dataset of aircraft-based immersion mode INP measurements and aerosol size-resolved composition in the Western North American Arctic from the 11<sup>th</sup> – 21<sup>st</sup> March 2018. Aerosol samples were collected between ~70 and 500 m above the surface on filters that were analysed using both a freezing droplet-based assay and Scanning Electron Microscopy with Energy Dispersive Spectroscopy (SEM-EDS). The measured INP concentrations were at or close to the limit of detection, with concentrations at -20°C of 1 L<sup>-1</sup> or below. The size-resolved composition measurements indicates that the aerosol concentrations were low, dominated mostly by sea spray aerosol and mineral dust. Further analysis shows that mineral dust is important for the ice-nucleating properties of our samples, dominating over the sea spray aerosol particles in the four cases we analysed, suggesting that mineral dust is a relevant source of INPs in the Alaskan springtime Arctic. Furthermore, the INP concentrations are more consistent with fertile soil dusts that have an ice active biological component than what would be expected for the ice-active mineral K-feldspar alone. While we cannot rule out local high latitude sources of dust, the relatively small size of the mineral dust implies that the dust was from distant sources.

## 1. Introduction

Clouds containing both supercooled liquid water and ice are known as mixed-phase clouds and they reflect a substantial amount of the incoming solar shortwave radiation that reaches the Earth {Boucher, 2013 #399}. The lifetime, as well as the amount of radiation that these clouds reflect, is strongly affected by the partitioning between liquid and ice {Storelvmo, 2015 #658}. When above temperatures required for homogeneous freezing (below ~-35°C), ice formation in mixed-phase clouds is initiated by the presence of a small fraction of the aerosol particles known as ice-nucleating particles (INPs) {Murray, 2012 #60}. Once ice crystals nucleate, they can grow more rapidly than liquid cloud droplets since ice has a lower equilibrium vapour pressure than supercooled water. This process can lead to the precipitation of the ice crystals, removing liquid water from a cloud {Korolev, 2017 #712; Vergara-Temprado, 2018 #408; Hawker, 2021 #792}. Ice-related processes in mixed-phase clouds such as the primary production of ice and the link to INP concentration are commonly oversimplified in climate models, which contributes to large discrepancies in the amount of water and ice that the models simulate {Komurcu, 2014 #767; McCoy, 2016 #761; McCoy, 2018 #622}. The difficulty of properly representing

45 the current water and ice mixing state of these clouds is responsible for the large uncertainty of the  
46 cloud-phase feedback {Storelvmo, 2015 #658}.

47 As the atmosphere warms, mixed-phase clouds will contain more supercooled water leading to a  
48 reduction in shortwave radiation reaching the surface, but also decrease the outgoing longwave radiation  
49 flux {Ceppi, 2017 #662; Murray, 2021 #783}. Hence, mixed-phase mid- to high-latitude clouds over the  
50 ocean have a negative feedback {Tan, 2016 #552}, whereas clouds over high albedo ice or snow  
51 covered surfaces have a positive feedback {Tan, 2016 #552}. The strength of these feedbacks depends  
52 on the balance between ice and supercooled water in these clouds both in the present and future climate.  
53 This is particularly important for boundary layer cold sector clouds in the oceanic mid- to high-latitudes.  
54 Hence, better understanding the sources and concentrations of atmospheric INPs, particularly at the  
55 mid- to high-latitudes could help to reduce the uncertainty associated with cloud-phase feedbacks.

56 Only a small fraction of aerosol particles have the potential to become INPs. Transported dust from the  
57 deserts is one of the most important sources of worldwide atmospheric INPs, especially at temperatures  
58 below -15 °C {Hoose, 2012 #317; Vergara-Temprado, 2017 #396; Kanji, 2017 #550}. Given the fact that  
59 substantial amounts of dust are transported from the deserts to the Arctic {Fan, 2013 #718; Huang, 2015  
60 #759; Francis, 2018 #760}, this dust could contribute to the INP population of the region {Irish, 2019  
61 #752; Yun, 2022 #828}. Additionally, local sources of high-latitude dust are known to contribute to the  
62 dust budget in the Arctic {Bullard, 2016 #569; Groot Zwaaftink, 2016 #570; Meinander, 2021 #824; Shi,  
63 2021 #826}. Some of these sources of high-latitude dust have been found to contribute to the Arctic  
64 INP population {Tobo, 2019 #588; Sanchez-Marroquin, 2020 #751; Si, 2019 #768}. A fraction the INP  
65 in the Arctic are also of biogenic origin {Wex, 2019 #736; Porter, 2022 #827}, some of which may be  
66 associated with biogenic material in sea spray and some of which may be from terrestrial sources  
67 {Wilson, 2015 #321; DeMott, 2016 #599; Vergara-Temprado, 2017 #396; Irish, 2017 #772; McCluskey,  
68 2018 #668; Bigg, 2001 #754; Creamean, 2019 #753; Hartmann, 2020 #755; Creamean, 2020 #834}.  
69 Biogenic material attached to dust particles could be an important part of these terrestrial INPs  
70 {O'Sullivan, 2014 #653; O'Sullivan, 2015 #676; Tobo, 2019 #588}. Other types of aerosol particles such  
71 as volcanic ash or biomass burning particles could also contribute to the INP population in the Arctic  
72 {Prenni, 2009 #769}.

73 The available literature data indicates that the INP concentrations in the Arctic are highly variable,  
74 depending on the season and location {Murray, 2021 #783}. Using samples from land-based sites  
75 around the Arctic collected over several years, {Wex, 2019 #736@@author-year} found that Arctic  
76 INP concentrations reach a minimum during winter, but they increase through spring and reach a  
77 maximum around the summer, suggesting that concentrations are highest when the transport of aerosol  
78 from the low latitudes is at its weakest (the summer). Similarly, year-round measurements in the central  
79 Arctic indicate peak concentrations in the summer months of 2020 {Creamean, 2022 #866},  
80 {Creamean, 2022 #866@@author-year} suggested that local Arctic marine sources might contribute to  
81 the elevated INP populations in the summer. {Porter, 2022 #827@@author-year} also found elevated  
82 summertime INP concentration, during August 2018, while in the pack ice near the North Pole.  
83 However, in contrast to {Creamean, 2022 #866@@author-year}, {Porter, 2022 #827@@author-year}  
84 used detailed back trajectory analysis to concluded that these very active INPs were associated with  
85 Measurements at the summertime North Pole indicate highly variable INP concentrations, with air  
86 masses that have spent the preceding week or so over ice-covered surfaces having very low INP particle  
87 concentrations, and air masses originating from lower latitude ice-free regions along the Russian coast,  
88 whereas air masses that had spent the preceding week or so over ice-covered surfaces (in the central  
89 Arctic pack ice) had very low INP particle concentrations having very high biological INP  
90 concentrations. The central Arctic in 2018 and 2020 appear to be rather different, with {Porter, 2022  
91 #827@@author-year} reporting up to 2 L<sup>-1</sup> at -15°C in 2018, whereas {Creamean, 2022  
92 #866@@author-year} reported two orders of magnitude lower peak INP concentrations in 2020. Hence,  
93 there may simply be a great deal of variability and the contrasting conclusions between {Porter, 2022

94 #827@@author-year} and {Creamean, 2022 #866@@author-year} may be appropriate for their  
95 respective study periods. {Creamean, 2018 #604@@author-year; Creamean, 2018 #604@@author-  
96 year} found a similar trend in INP concentrations to {Wex, 2019 #736@@author-year} over spring,  
97 with coarse particles being responsible for the higher INP concentration event. However, a recent study  
98 did not find strong seasonality of Arctic INPs at Ny-Ålesund, although these measurements were  
99 limited to being between April and August 2018 {Rinaldi, 2021 #756}. Furthermore, there have been  
100 very few INP measurements from aircraft. Given there are strong aerosol sinks in the boundary layer,  
101 whereas the air above the boundary layer can be stratified with corresponding long aerosol lifetimes  
102 {Carslaw, 2022 #857}, vertical measurements are required. {Hartmann, 2020 #755} report INP spectra  
103 for late March and early April north of 80° over the Fram Strait and Arctic Ocean and report that the  
104 highest INP concentrations ( $2 \times 10^{-2} \text{ L}^{-1}$  at  $-15^\circ\text{C}$ ) correspond to the boundary layer, indicating a local  
105 marine source even though the region was mostly ice covered. Overall, the picture of INP concentrations  
106 in the Arctic is that of high variability, both spatially and temporal (on days to years timescales), with  
107 the potential for high variability in local sources, transport from lower latitudes as well as in local INP  
108 sinks.

109 ~~Although substantial amounts of anthropogenic pollutants exist in the Arctic during the spring, they do~~  
110 ~~not seem to significantly contribute to the INP concentration~~ {Creamean, 2018 #604; Borys, 1989  
111 #745}. ~~Measurements at the summertime North Pole indicate highly variable INP concentrations, with~~  
112 ~~air masses that have spent the preceding week or so over ice covered surfaces having very low INP~~  
113 ~~particle concentrations, and air masses originating from lower latitude ice free regions along the~~  
114 ~~Russian coast having very high biological INP concentrations~~ {Porter, 2022 #827}.

115 In this paper, we present a set of immersion mode INP and aerosol size-resolved composition  
116 measurements carried out in the Western North American Arctic during March 2018 using an aircraft.  
117 INP measurements were combined with aerosol characteristics determined using SEM-EDS to indicate  
118 the types of INPs that were most important during this campaign.

119

## 120 2. Sampling location and methods

121 Aerosol particles were sampled from the UK's BAe-146 FAAM atmospheric research aircraft during  
122 the Measurements of Arctic Cloud, Snow and Sea Ice in the Marginal Ice Zone (MACSSIMIZE)  
123 campaign, based in Fairbanks, Alaska (US) in March 2018. The majority of the measurements were  
124 carried out close to the northern coast of Alaska and the Canadian territory of Yukon, both over land  
125 and over the Arctic Ocean, as shown in Fig. 1, where the approximated midpoint of the filter sampling  
126 run locations are shown with a star. Measurements were carried out at altitudes between 40 and 600 m  
127 above sea level, as detailed in Table 1 along with other pertinent information. Some filters were  
128 collected in a single run on a constant heading and height, while others were collected over several runs,  
129 with the filters system mostly closed during turns between the runs and altitude changes, although this  
130 was not possible for all filters. Filters were collected over 9 to 36 minutes, which at a science speed of  
131 ~360 km hr<sup>-1</sup> corresponded to a horizontal distance of between ~50 and ~200 km. The sampling  
132 locations as well as sampling altitudes are shown in Fig. 1. All the sampling was done outside of cloud  
133 and precipitation.

134 Additionally, the Hybrid Single-Particle Lagrangian Integrated Trajectory (HYSPPLIT) model was used  
135 to calculate five-day back trajectories of sampled air masses {Stein, 2015 #818; Rolph, 2017 #819} and  
136 shown in Fig. 1. The back trajectories show that in most cases air masses remained near or over Alaska  
137 and northern Canada before sampling. For 13 of the 16 samples, the trajectories indicate that the air  
138 mostly stayed at altitudes below 1000 m above sea level in the five days prior to sampling. At the time  
139 of sampling, most of the sea and land surfaces were covered by sea ice or snow (Fig. 1), which most  
140 likely suppressed any local aerosol sources.

141 Aerosol particles were collected using the filter inlet system on board of the FAAM BAe-146, which  
142 has been characterised by {Sanchez-Marroquin, 2019 #598@author-year}. Briefly, this inlet is  
143 located outside the skin of the FAAM BAe-146 and brings aerosol particles to a filter located inside the  
144 cabin with a 45° angle bend. The sampling occurs in sub-isokinetic conditions, which enhances coarse  
145 mode aerosol particles. Sampling efficiency for particles with diameters above 20 µm becomes very  
146 small due to inertial losses in the system (at the bend). No treatment (heat or drying) is applied to the  
147 sampled air mass, although the cabin was warmer than the ambient air in this campaign and hence the  
148 RH of air passing through the inlet system once inside the aircraft is therefore very low. The system  
149 allowed us to collect two aerosol samples in parallel: one on a polycarbonate filter (Whatman Nuclepore  
150 polycarbonate track-etched filters, 47 mm diameter with a pore size of 0.4 µm) and one on a Teflon  
151 filter (Sartorius polytetrafluoroethylene, 47 mm diameter with a pore size of 0.45 µm). For these filter  
152 types, the particle collection efficiency is likely to be close to 100 % for the relevant size ranges, as  
153 discussed in {Sanchez-Marroquin, 2019 #598@author-year} using the data of {Soo, 2016  
154 #462@author-year} and {Lindsley, 2016 #415@author-year}.

155 The ice-nucleating particle assay was conducted in a temporary laboratory set up in a hotel room near  
156 the aircraft base in Fairbanks, Alaska, with minimum time between sampling and analysis. Most filters  
157 were analysed a matter of hours after collection, however where this was not possible they were stored  
158 at ~ -18 °C for a few days prior to analysis. This approach has a number of advantages compared to the  
159 commonly used strategy of bringing filters back to a laboratory for latter analysis. Firstly, analysis of  
160 field blanks can reveal sources of contamination that can be reduced by making adjustments to the  
161 experimental protocol; secondly, we can try to adjust the sampling methodology (such as sampling  
162 time) to fit the INP concentration and thirdly, we can minimise storage and transport of filters thus  
163 reducing potential biases. Teflon filters were used to perform a droplet-on-filter freezing assay to  
164 quantify the INP concentration, as described in detail in {Price, 2018 #450@author-year} and also  
165 used by {Sanchez-Marroquin, 2020 #751@author-year} and {Sanchez-Marroquin, 2021 #750}. The  
166 technique was first described by {Schnell, 1982 #620@author-year} and our version of this assay  
167 makes use of the Asymptote EF600 Stirling cooler described in {Whale, 2015 #293@author-year}.



168 For the present study we pipetted 2  $\mu$ L pure water droplets on top of each filter that had been exposed  
169 to aerosol particles (or handling blanks). On average, we pipetted 54 (with and standard deviation of 5)  
170 droplets per filter. The filters were placed on top of a cold stage, within a chamber that is flushed with  
171 dry nitrogen gas to prevent water condensation, that is cooled at a constant rate of  $1\text{ }^{\circ}\text{C}/\text{min}^{-1}$  until  
172 temperatures of  $\sim 35\text{ }^{\circ}\text{C}$ . Droplet freezing was recorded and the resulting videos were manually  
173 analysed to determine the fraction of droplets frozen at each temperature and then the INP  
174 concentration. At least one handling blank experiment was performed for every flight. Handling blank  
175 filters were prepared and transported in the same way as the measurement filters including loading the  
176 filters into the sampling system on the aircraft and briefly opening (for a second or so) and closing the  
177 inlet valves that allow air to pass through the filters. Hence, the handling blank should provide  
178 information on sources of contamination throughout the handling of the filter. A disadvantage of the  
179 droplet-on-filter technique is that each sample can only be analysed once, which makes it incompatible  
180 with standard heat tests such as the ones analysed in described by {Daily, 2022 #867@ @author-year}.  
181 However, the great advantage of the droplet-on-filter technique over techniques where particles are  
182 washed off a filter into a volume of water is that it is around 20 times more sensitive than a typical  
183 wash-off assay employing 1  $\mu$ L droplets (depending on the details of the freezing assays). This  
184 enhanced sensitivity is very important given that aerosol sampling durations are typically only a few  
185 tens of minutes long.

186 The droplet fraction frozen (the fraction of droplet that were frozen as a function of temperature)  
187 produced by our samples, along with those produced by the handling blank filters, is shown in Fig 2a.  
188 While the fraction frozen for the sample filters were generally shifted to warmer temperatures than the  
189 handling blanks, many of the samples overlapped with the range defined by the handling blanks. Hence  
190 it was necessary to account for influence of the background from the measurements. The background  
191 subtraction procedure and the INP concentration calculations are detailed in Appendix A. Briefly, we  
192 converted our cumulative fraction frozen values for the samples and handling blanks into the differential  
193 INP spectrum,  $k(T)$ , in units of INP per unit temperature {Vali, 1971 #284; Vali, 2019 #757}.  $k$  is the  
194 number of INP that become active in a temperature interval. This allowed us to define a limit of  
195 detection then apply a criterion to separate samples that show a significant signal above this from the  
196 ones that do not. Data points whose error bars did not overlap with the error bars associated to the  
197 handling blank were considered to be above the limit of detection. The error bars of the differential  
198 concentrations of the samples represent a confidence level of 68 % while the error bars of the  
199 background represents the standard deviation of all the measured handling blanks. Background-  
200 subtraction was applied to data points above the limit of detection ( $k_{\text{sample}} - k_{\text{background}}$ ) using a similar  
201 approach to {Vali, 2019 #757@ @author-year}. The cumulative INP spectrum, the common way of  
202 presenting INP data, was then derived using the background corrected values of  $k$ .

203 A subset of the polycarbonate filters was analysed using Scanning Electron Microscopy with Energy  
204 Dispersive Spectroscopy (SEM-EDS) to study aerosol size-resolved composition. The analysis was  
205 carried out in the Leeds Electron Microscopy And Spectroscopy centre (LEMAS), at the University of  
206 Leeds. Filters were transported to the University of Leeds and then stored at  $\sim -18\text{ }^{\circ}\text{C}$  until its analysis.  
207 This technique can be used to obtain the morphological and chemical properties of individual aerosol  
208 particles within the sample. The subset of samples was coated with a 30 nm layer of Iridium and the  
209 SEM-EDS analysis was performed using an accelerating voltage of 20 KeV. The scanning and  
210 acquisition of EDS spectrums is done using a semi-automatic method with the Aztec Feature Software  
211 by Oxford Instruments. Our method captures the morphology and chemical signature of particles down  
212 to 0.2 or 0.3  $\mu\text{m}$ , depending on the sample. Particles are detected based on their contrast in the secondary  
213 electron images, although some artefacts were removed manually. Each particle is then classified into  
214 a defined composition category based on its chemical composition. The morphological and composition  
215 category of each particles is used to obtain statistics about the size-resolved composition of the aerosol  
216 samples. A more detailed description of the technique can be found in {Sanchez-Marroquin, 2019  
217 #598@ @author-year}.

218 In parallel with the filters sampling, we make use of FAAM's underwing optical particle counters. One  
219 of these counters is the Passive Cavity Aerosol Spectrometer Probe 100-X (PCASP), manufactured by  
220 Particle Measurement Systems, and measures aerosol particles in the 0.1 to ~3  $\mu\text{m}$  range. The second  
221 counter is the Cloud Droplet Probe (CDP) by Droplet Measurement Technologies and it measures  
222 aerosol particles and droplets with sizes from ~3 to 50  $\mu\text{m}$ . A detailed description of these instruments  
223 and its calibration and can be found in {Rosenberg, 2012 #456@-year }.

224 The Hybrid Single-Particle Lagrangian Integrated Trajectory (HYSPLIT) model was used to calculate  
225 five day back trajectories of sampled air masses {Stein, 2015 #818;Rolph, 2017 #819} and shown in  
226 Sect S1. The back trajectories show that in many cases air masses remained near or over Alaska and  
227 northern Canada before sampling. However, the backtrajectories corresponding to the C085 flight  
228 arrived mostly from the south west. Most of the trajectories suggest that the air mostly stayed at altitudes  
229 below 1000 m above sea level in the five days prior to sampling. At the time of sampling, most of the  
230 sea and land surfaces were covered by sea ice or snow (Fig. 1), which most likely suppressed any local  
231 aerosol sources. However, local sources of marine aerosol particles may still occur due to open leads  
232 {May, 2016 #873;Kirpes, 2019 #758;Chen, 2022 #869}.

### 234 3. INP concentrations in the Western North American Arctic

235 The background corrected cumulative INP concentrations are shown in Fig 2b. Hollow markers indicate  
236 measurements consistent with the limit of detection, where the lower error bar goes to zero, while filled  
237 markers correspond to a cumulative INP concentration above the limit of detection. Using a 68 %  
238 confidence interval, approximately 70 % of the differential spectra binned data was not significantly  
239 above the limit of detection and around half of the data points in the cumulative INP spectra shown in  
240 Fig. 2b show INP concentrations consistent with zero (i.e. not above the detection limit). The reported  
241 INP concentrations are always below 0.1 and 1  $\text{L}^{-1}$  at -15  $^{\circ}\text{C}$  and -20  $^{\circ}\text{C}$ , respectively. However, given  
242 the fact that a substantial percentage of the data is not above the detection limit, the real values of some  
243 of these samples may be well below these values. A daily, more detailed representation of the INP  
244 concentrations is shown in Fig. B3.

245 INP concentrations across the Arctic vary significantly depending on the time of the year and location  
246 (Creamean et al., 2018;Si et al., 2019;Wex et al., 2019). Hence, in order to compare to the pertinent  
247 data we show our INP concentrations alongside literature data collected in a similar location and time  
248 of the year in Fig. 3 (we restricted the literature datasets from February to April). Some of our reported  
249 INP concentrations are above some of the values measured using a droplet freezing assay on filters  
250 collected the surface by Creamean et al. (2018) and, Wex et al. (2019) as well as filters collected on an  
251 aircraft and processed using a dynamic developing chamber at water saturation by Borys (1989).  
252 Creamean et al. (2018) reported INP concentrations at -20  $^{\circ}\text{C}$  up to 0.01  $\text{L}^{-1}$  on the north coast of Alaska  
253 in March. Measurements performed by Wex et al. (2019) in a close location (Utqiagvik) indicate that  
254 INP concentrations ranging from  $\sim 10^{-4}$  to  $10^{-2}$   $\text{L}^{-1}$  at -10  $^{\circ}\text{C}$  in March. The more active samples reported  
255 by Wex et al. (2019) form a consistent INP spectrum with our more active samples, but unfortunately  
256 there is no direct overlap. Borys (1989) reported INP concentrations of 0.001  $\text{L}^{-1}$  to 0.3  $\text{L}^{-1}$  at -25  $^{\circ}\text{C}$   
257 measured from an aircraft at a similar location and time of the year. These values are of course consistent  
258 with our samples where we report upper limits, but some of our samples clearly had substantially higher  
259 INP concentrations than the range reported by Borys (1989). Hiranuma et al. (2013) also report INP  
260 measurements using an airborne continuous flow diffusion chamber (CFDC) during the Indirect and  
261 sSemi-dDirect aAerosol eCampaign (ISDAC) in a very similar study region to ours, but in April rather  
262 than March. We have only compared our measurements with theirs at water saturation, which happened  
263 to be during a relatively high INP period. This INP value of  $5.6 \pm 3.5$   $\text{L}^{-1}$  at -22 $^{\circ}\text{C}$  is consistent with our  
264 highest recorded INP concentrations. Overall, this comparison with measurements in previous years at  
265 a similar location and time of year indicates that the INP concentrations are rather variable, ranging

266 ~~over at least three orders of magnitude at -20°C. Although the literature INP concentrations have been~~  
267 ~~measured in close locations at a similar time of the year than the ones reported in this study, the~~  
268 ~~measurements were performed in different years when the INP population may have been different.~~

269 Our measurements have also been presented alongside a compilation of INP measurements from across  
270 the Arctic carried out throughout the year (Fig 3b). Our dataset is well within the range of literature INP  
271 measurements from across the Arctic. Around 50% of our data points were below detection limit (and  
272 not shown in Fig. 3), hence we are only able to report INP concentrations when their values are  
273 relatively high. The picture that emerges in the Arctic is a region of highly variable INP concentrations.  
274 This variability is likely related to a combination of transport from local and remote sources of INP as  
275 well as sinks both locally and along those transport routes. This high variability in INP concentrations  
276 will affect primary ice production in clouds, with more INP leading to greater ice concentrations that  
277 may or may not be amplified by secondary production processes. Intriguingly, several authors report  
278 that greater INP concentrations leads to more ice in Arctic cloud and vice versa (Rogers et al.,  
279 2001;Hiranuma et al., 2013).

280 A handful of measurements of INP have been made from aircraft (Hartmann et al., 2020;Sanchez-  
281 Marroquin et al., 2020;Prenni et al., 2009) and it is these measurements that produce many of the highest  
282 observed Arctic INP concentrations, rather than those made on the ground. However, aircraft sampling  
283 is often limited by the volume of air that can be sampled due to restrictions in flight lengths and other  
284 technical limitations. This necessarily biases the results to relatively high INP concentrations. For  
285 example, (Rogers et al., 2001) report that 50% of the 10 s averaged data was zero (i.e. below detection  
286 limit).- Given the Arctic atmosphere is highly stratified, it would be interesting to perform simultaneous  
287 measurements at the surface and from an aircraft to explore how or if INP at the surface are related to  
288 those higher in the boundary layer and those in the free troposphere.

#### 289

#### 290 **3.4. SEM-EDS size-resolved composition analysis**

291 The equivalent circular diameter size distributions obtained with the SEM-EDS technique were  
292 compared with the average size distributions for the same sampling periods measured using the  
293 underwing optical particle counters on-board of the FAAM BAe-146. The analysis is shown in Fig. 4  
294 alongside the size-resolved chemical composition of the analysed samples. The number size distribution  
295 is multiplied by the fraction of particles in each category and binned to calculate the number size  
296 distribution of each category. Then these number size distributions are turned into surface area size  
297 distributions and integrated to obtain the surface area of each category, as shown in Table 2.

298 The analysed samples exhibited low aerosol concentrations relative to other locations where we have  
299 used this technique, especially for the coarse mode. In this study, almost no particles above 10  $\mu\text{m}$  were  
300 detected, in contrast to samples from around Iceland, the eastern tropical Atlantic and the south east of  
301 the United Kingdom analysed using the same or similar technique, where significant amounts of  
302 aerosols in between 10 and 20  $\mu\text{m}$  were detected (Price et al., 2018;Sanchez-Marroquin et al.,  
303 2019;Sanchez-Marroquin et al., 2020;Sanchez-Marroquin et al., 2021). Most of the detected particles  
304 were below  $\sim 2 \mu\text{m}$ . At sizes below  $\sim 3 \mu\text{m}$ , the comparison between the optical probes and the SEM-  
305 EDS size distributions are consistent in most cases, with an undercounting at the lower end of the SEM-  
306 EDS technique ( $\sim 0.3 \mu\text{m}$ ). This undercounting is related to the difficulty in observing small organic rich  
307 particles and has been discussed in Sanchez-Marroquin et al. (2019). At sizes above  $\sim 3 \mu\text{m}$ , the optical  
308 probes and SEM-EDS size distributions showed a comparable amount of detected particles in samples  
309 C089\_3 and C090\_1. However, for samples C087\_1 and C091\_2, the optical counters detected a larger  
310 concentration of particles with sizes  $\sim 5$  to 10  $\mu\text{m}$  than the SEM analysis of the filters. Similar  
311 discrepancies have been observed previously with these instruments in another low aerosol environment  
312 (Young et al., 2016), and were attributed to regions of high humidity even if the average humidity in a

313 run should not have led to substantial hygroscopic growth. In dust plumes near Iceland and in aerosol  
314 around the UK where there was a significant coarse mode the agreement between CDP and SEM tended  
315 to be good. We note CDP is designed for cloud droplets, and we are using it at the edge of its capability  
316 for larger aerosol particles, hence there may be some biases which seem more significant in low aerosol  
317 environments. Furthermore, for these two samples, the optical size distribution above  $\sim 3 \mu\text{m}$  has shape  
318 that is atypical of atmospheric aerosol size distributions (the aerosol concentration drops about 4 orders  
319 of magnitude from  $\sim 5$  to  $\sim 10 \mu\text{m}$ ). As a consequence, it is very likely these parts of the size distribution  
320 measured by the optical probes are produced by artefacts such as cloud droplets rather than representing  
321 the actual aerosol concentration at that location.

322 In terms of chemical composition, the samples were mainly dominated by sea spray (Na rich) and  
323 mineral dust (Si rich, Si only, Al-Si rich and Ca rich) particles. There were some smaller contributions  
324 of S rich particles (likely sulphates) and Carbonaceous particles (likely black carbon or organic  
325 material). This is consistent with other SEM-EDS studies of the aerosol samples collected on the  
326 Alaskan Arctic from the ground (Chen et al., 2022; Creamean et al., 2018; Kirpes et al., 2018; Gunsch et  
327 al., 2017) or during a ship campaign (Kirpes et al., 2020). However, we tend to observe larger fractions  
328 of dust aerosol particles, particularly in the sample C090\_1, where this type of aerosol constituted  $\sim 65$   
329 % of the surface area of the sample.

330 In this dataset, nearly all particles in the Na rich category were dominated by the presence of Na and  
331 Cl, having traces of other elements (such as S in some occasions), consistent with sea spray particles.  
332 As a consequence, we will refer to particles in this category as sea spray aerosol particles. Some  
333 carbonaceous particles were also detected through most sizes and there were significant contributions  
334 of S rich aerosol, particularly in the accumulation mode. As shown in Fig. 4 and Table 2, the surface  
335 area of samples C087\_1 and C091\_2 were dominated by sea spray aerosol particles with sizes around  
336  $\sim 1 \mu\text{m}$ . In Sect. S1 it is shown that most of the air masses associated with these samples had been  
337 circulating above the Arctic Ocean at relatively low altitude (below 1000 m) before sampling took place.  
338 This is consistent with the fact that sea spray aerosol particles are normally emitted by bubble bursting  
339 in the surface of the oceans (Lewis and Schwartz, 2004). It is possible that the detected sea spray aerosol  
340 in our study was transported from ice free oceans. However, Sect. S1 indicates that the closest ocean  
341 masses were almost fully covered by sea ice (with some open leads) during the campaign and the  
342 majority of the sampled air masses did not pass by the open oceans prior to sampling. Hence, it is very  
343 likely possible that the sea spray particles had been emitted from open leads in the sea ice, as this is  
344 thought to be a common source of sea spray aerosol in the region (May et al., 2016; Kirpes et al.,  
345 2019; Chen et al., 2022). It is also possible that some of the sea spray aerosol has been directly emitted  
346 from the sea ice through blowing snow events (Yang et al., 2008; Huang and Jaeglé, 2017; Frey et al.,  
347 2020).

348 Particles in the categories Si rich, Si only, Al-Si rich and Ca rich have a chemical composition consistent  
349 with mineral dust particles so we will refer to them collectively as mineral dust. However, it should be  
350 borne in mind that the composition of particles in these categories is also consistent with some types of  
351 combustion ashes or volcanic ash. Mineral dust particles were present in all the samples, particularly  
352 with sizes between 1 and  $5 \mu\text{m}$ , constituting a substantial percentage of its surface area, as shown in  
353 Table 2. This was particularly the case in the sample C090\_1, where 65 % of the surface area was given  
354 by mineral dust particles. Although we cannot fully determine the relative contribution of different  
355 sources to the detected mineral dust, several arguments suggest that the sampled mineral dust originated  
356 from the low latitude deserts. The back trajectory analysis shown in Sect. S1 suggests that most of the  
357 air masses had been circulating around the sampling location prior to sampling for  $\sim 5$  days and the  
358 C090\_1 sample air had passed across the north coast of Alaska. However, the majority of the potential  
359 high-latitude dust sources were covered by snow at this time, so it seems unlikely that this mineral dust  
360 is related to natural emissions, although we cannot rule out sources associated with human activities  
361 along the coast (e.g. Purdue Bay oil fields). Mineral dust originating from the Sahara and Central Asia



362 is known to be transported to the Arctic, especially in late winter and early spring, when this study took  
363 place (VanCuren et al., 2012; Fan, 2013; Huang et al., 2015; Francis et al., 2018; Shi et al., 2022; Zhao et  
364 al., 2022). This is consistent with the some of the backtrajectories associated to the samples collected  
365 on the C085 flight, which originate from Asia. Almost all the mineral dust particles found in this study  
366 had sizes below 5  $\mu\text{m}$  and it is known that dust particles have a lifetime of many days so can conceivably  
367 be transported to Alaska from distant sources (Huneeus et al., 2011; Ménégos et al., 2012). Once in the  
368 Arctic, accumulation mode aerosol has a lifetime extending to months during winter and spring, when  
369 removal processes are weak {Carslaw, 2022 #857}. The small sizes of dust particles found in this  
370 campaign contrast with results obtained using similar techniques on samples collected closer to dust  
371 sources, where dust particles with sizes above 10  $\mu\text{m}$  are frequent (Price et al., 2018; Ryder et al.,  
372 2018; Sanchez-Marroquin et al., 2020). Although this evidence suggests that most of our dust likely  
373 originated in arid lower-latitude deserts, high-latitude dust could still contribute to the dust budget or  
374 even dominate it during other times of the year such as autumn (Groot Zwaafink et al., 2016).

375 As shown in Table 2, C087\_1 and C091\_2 samples have a larger surface area of sea spray aerosol  
376 particles (Na rich) than mineral dust, whereas sample C090\_1 is dominated by the presence of mineral  
377 dust. Hence, it is reasonable to ask if the mineral dust or organic material associated with sea spray is  
378 the more important INP type in these samples. To estimate the relative contribution of mineral dust and  
379 sea spray aerosol to the INP population, we present the expected INP concentrations based on the SEM-  
380 EDS surface areas in Fig. 5, in comparison with the measured INP concentrations. The INP  
381 concentrations expected from the SEM-EDS analysis were calculated assuming a dust containing 10 %  
382 of K-feldspar (Harrison et al., 2019) (the ice active component of desert dust) and the parametrization  
383 of fertile soils given by O'Sullivan et al. (2014). Note that the latter is very similar to the desert dust  
384 parameterization given by Ullrich et al. (2017). For the pristine sea spray INP, the parametrization given  
385 by McCluskey et al. (2018) that links INP concentration and aerosol surface area has been used. As  
386 shown, even in the cases where there is more sea spray aerosol than mineral dust (C087\_1 and C091\_2),  
387 the minimum contribution of mineral dust INP is orders of magnitude above the INPs produced by the  
388 pristine sea spray aerosol particles. It is possible that the sea spray in this location was more active than  
389 defined by McCluskey et al. (2018), however, the INP concentrations calculated based on the presence  
390 of dusts better explains the observed INP concentrations measured using the droplet freezing assay at  
391 the lower end of the temperature spectrum. At the higher end of the temperature spectrum, the measured  
392 INP concentrations are above those expected from a 10 % K-feldspar dust, but are consistent with the  
393 fertile soil dust parameterisation. It is known that fertile soil dusts contain biological ice nucleating  
394 material (O'Sullivan et al., 2014), hence this suggests that the samples from Alaska contained some  
395 biological ice nucleating material (either from marine or terrestrial sources). Although our INP  
396 concentrations would also be comparable with those predicted using the desert dust parameterization  
397 by Ullrich et al. (2017), the latter is usually higher than the activity of samples of airborne desert dust  
398 at temperatures greater than about  $-20^{\circ}\text{C}$  from other studies (Boose et al., 2016; Price et al.,  
399 2018; Harrison et al., 2022; Reicher et al., 2018; Gong et al., 2020). It has been suggested that dust that  
400 has been transported far from its source regions is less active than arid soil dusts that have been recently  
401 aerosolised and also there appears to be substantial differences in activity of dust from different source  
402 regions (Boose et al., 2016; Harrison et al., 2022). Hence, we suggest that the enhanced ice-nucleation  
403 ability of our samples is perhaps due to the presence of biological material. This is consistent with other  
404 studies thatwhe also provideds evidence that Arctic INP samples have a substantial biological  
405 component (Wex et al., 2019; Creamean et al., 2019; Santl-Temkiv et al., 2019; Porter et al., 2022).

406  
407

#### 4.5. Conclusions

408 In this study, we present a new dataset of INP and SEM-EDS aerosol size-resolved composition  
409 measurements in the Western North American Arctic in March 2018. Back trajectory analysis suggests  
410 that most of these air masses spend the preceding five days circulating over or near Alaska and Northern

411 Canada where local sources of primary aerosol were suppressed by snow and ice cover. Observed INP  
412 concentrations were at or close to the limit of detection of the measuring technique, being always below  
413 0.1 and 1 L<sup>-1</sup> at -15 °C and -20 °C respectively. SEM-EDS analysis revealed that samples are mostly  
414 dominated by the presence of mineral dust and sea spray aerosol particles, with some contributions of  
415 sulphur rich and carbonaceous particles. The mineral dust is most likely sourced from the low-latitudes,  
416 rather than local high-latitude dust sources. Our analysis shows that mineral dust will always contribute  
417 more INP to the INP population than sea spray, despite sea spray being more abundant in some samples.  
418 However, it appears that the ice-active mineral K-Feldspar cannot account for all of the observed INPs,  
419 especially above ~ -22°C. This suggests that there is another INP type that controls the INP spectrum  
420 above -22°C; these particles may be biogenic in origin, but where this biogenic ice nucleating material  
421 might be derived from is unclear. More work is clearly required to understand the sources and nature  
422 of INP in the winter and early springtime Arctic.

423 **Acknowledgments**

424 We are grateful to all the people involved in the MACSSIMIZE campaign, led by Chawn Harlow (UK  
425 Met Office). The samples were collected using the FAAM BAe-146-301 Atmospheric Research  
426 Aircraft, flown by Airtask Ltd., maintained by Avalon Aero Ltd., and managed by FAAM Airborne  
427 Laboratory, jointly operated by UKRI and the University of Leeds. We acknowledge the Centre for  
428 Environmental Data Analysis for the access to the FAAM datasets used here. We would also like to  
429 thank Duncan Hedges and Richard Walshlaw at the Leeds Electron Microscopy and Spectroscopy  
430 Centre.

431

432 **Author contributions**

433 Aerosol measurements during the MACSSIMIZE campaign were organised by ASM, JBM, and BJM.  
434 ASM and BJM worked on the manuscript with contributions from all authors. The field work was  
435 carried out by ASM and JBM. ASM performed all the experimental measurements (INP analysis and  
436 SEM-EDS). The SEM-EDS technique was developed by ASM and ITB. The back-trajectory analysis  
437 was carried out by SLB and ASM. All the authors contributed to the discussion.

438

439 **Financial support**

440 This research has been supported by the European Research Council (MarineIce (grant no. 648661))  
441 and the Natural Environment Research Council (NE/R006687/1, NE/T00648X/1).

442

443 **Competing interests**

444 The authors declare that they have no competing interests.

445

446 **Data and materials availability**

447 All data needed to evaluate the conclusions in the paper are present in the paper and/or the  
448 Supplementary Materials. The digitalized data are available from <https://doi.org/xx.xxxx/xxx>. FAAM  
449 data associated to the flights can be found in: Facility for Airborne Atmospheric Measurements; Natural  
450 Environment Research Council; Met Office (2018): FAAM C085 MACSSIMIZE flight: Airborne  
451 atmospheric measurements from core and non-core instrument suites on board the BAE-146 aircraft.  
452 Centre for Environmental Data Analysis.  
453 <https://catalogue.ceda.ac.uk/uuid/b04281cc10c44d9dab1eb2e4eb19d5b8>.

454

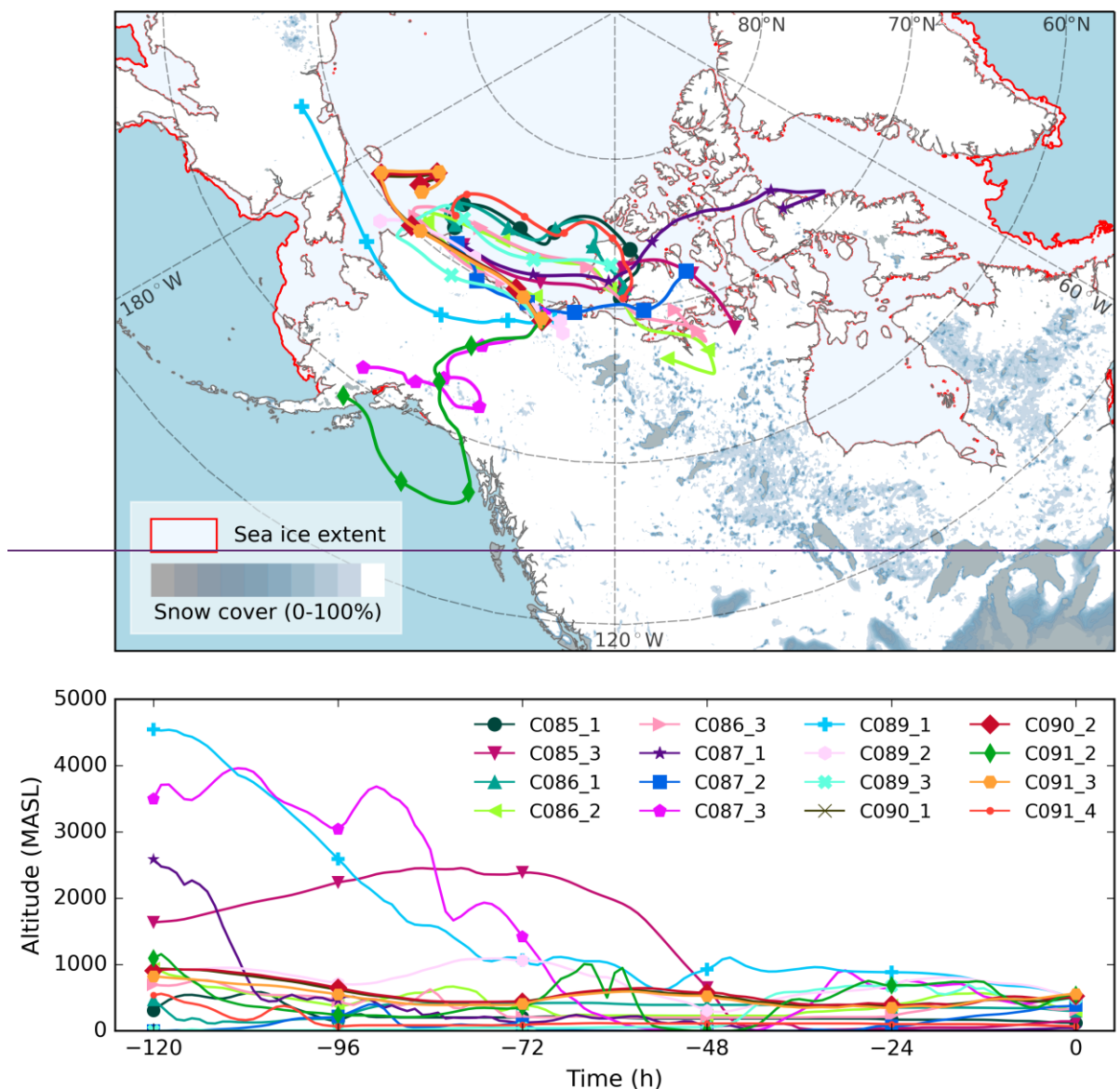
455

<u>Sample</u>	<u>Date (2018)</u>	<u>Start time (UTC)</u>	<u>End time (UTC)</u>	<u>GPS altitude (m)</u>	<u>Radar altitude (m)</u>	<u>BL or FT</u>	<u>Vol. PC (L)</u>	<u>Vol. tef. (L)</u>	<u>PTFE position</u>	<u>Stored</u>	<u>Temperature (°C)</u>	<u>Dew temperature (°C)</u>	<u>Aerosol concentration (cm<sup>-3</sup>)</u>
C085_1	03/11 <sup>th</sup>	22:22	22:34	475	474	FT	466	312	Up	No	-11.1	-14.4	-
C085_3	03/11 <sup>th</sup>	23:18	23:40	604	546	FT	461	355	Low	No	-5.4	-10.6	-
C086_1	03/13 <sup>th</sup>	21:14	21:22	38	38	BL	212	159	Low	No	-16.8	-	76.4
C086_2	03/13 <sup>th</sup>	21:29	21:49	138	139	BL	231	143	Up	No	-17.9	-18.3	75.9
C086_3	03/13 <sup>th</sup>	22:11	22:31	386	387	Intersection	644	209	Low	No	-11.3	-14.1	35.3
C087_1	03/16 <sup>th</sup>	20:44	21:26	310	309	BL	1047	565	Low	No	-19.7	-	68.9
C087_2	03/16 <sup>th</sup>	21:33	22:03	304	305	BL	965	447	Up	No	-16.4	-	61.2
C087_3	03/16 <sup>th</sup>	22:30	22:44	536	491	FT	392	217	Low	Yes	-13.6	-	46.8
C089_1	03/18 <sup>th</sup>	18:01	18:42	584	522	FT *	1198	714	Low	No	-21.3	-20.2	40.3
C089_2	03/18 <sup>th</sup>	18:49	19:17	573	506	FT *	-	398	Low	No	-21.2	-19.3	45.2
C089_3	03/18 <sup>th</sup>	19:28	19:48	591	557	FT *	404	214	Up	Yes	-20.9	-18.8	47.7
C090_1	03/20 <sup>th</sup>	20:15	20:38	547	487	FT *	735	349	Low	No	-15	-15.4	62.1
C090_2	03/20 <sup>th</sup>	20:53	21:26	563	503	FT *	488	409	Up	No	-14.6	-15.6	62.3
C091_2	03/21 <sup>th</sup>	18:27	18:56	122	123	FT *	1187	376	Up	No	-28	-	63.6
C091_3	03/21 <sup>th</sup>	19:01	19:14	295	297	FT *	644	203	Low	Yes	-25.7	-	63.9
C091_4	03/21 <sup>th</sup>	19:21	19:51	71	68	FT *	635	635	Up	No	-29.8	-27.4	31.8

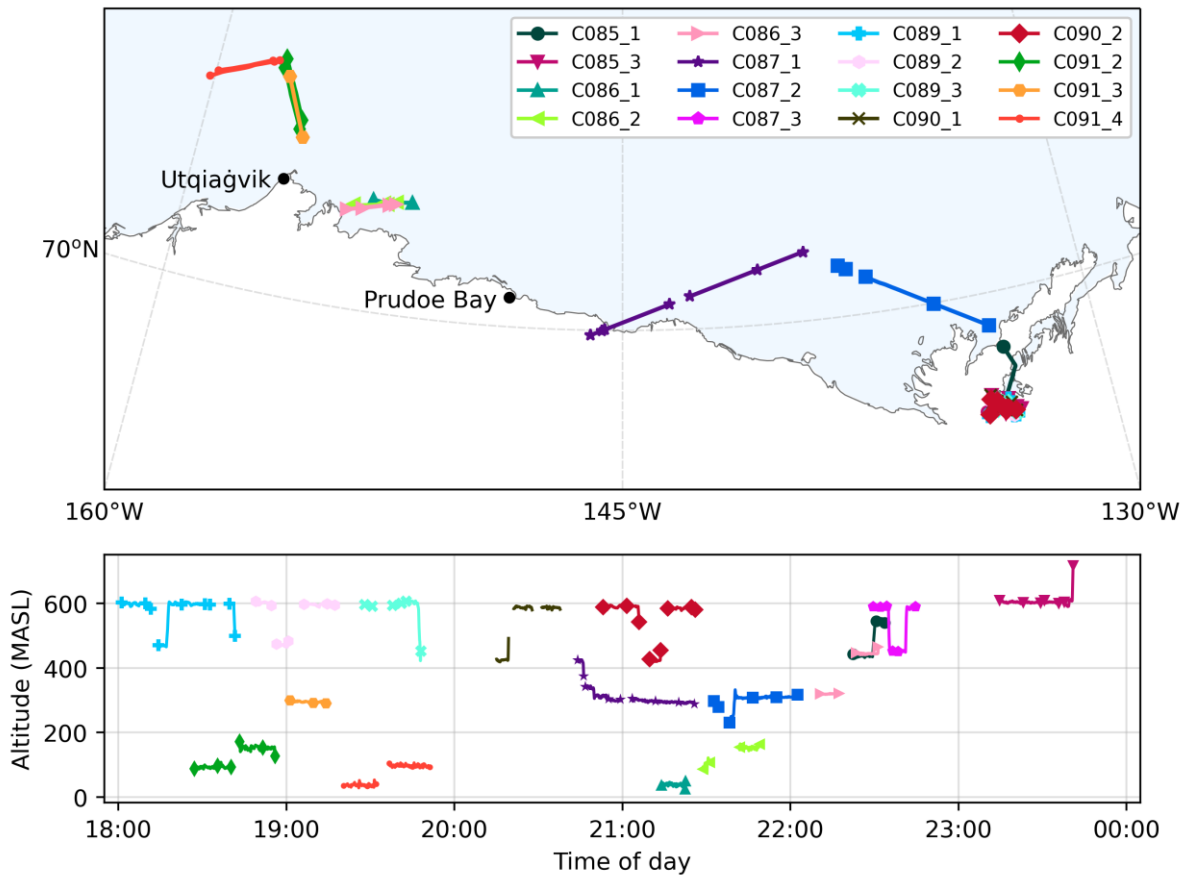
456 Table 1. Details of the samples collected during the MACSSIMIZE campaign. PTFE position  
457 refers to which inlet was used to collect the PTFE sample in each run. The other line was used  
458 to collect the polycarbonate sample. In order to determine if the sample was collected within  
459 the boundary layer (BL) or in the Free Troposphere (FT), we looked at the temperature and  
460 potential temperature profiles. (\*) For all the runs in the C089, C090 and C091, the flight did  
461 not descend low enough to determine the exact depth of the BL. Hence, it was assumed that  
462 the runs occurred above the BL. Stored filters were kept for a few hours or days at -18 °C,  
463 while the rest of them were analysed immediately after collection without any long-term  
464 storage. The given altitude values correspond to the average of each run. The mean values of  
465 the air temperature across the run was derived from the Rosemount de-iced temperature  
466 sensor, while the dew temperature is given by the Buck CR2 Hygrometer of the BAe-146.  
467 Dew temperature could not be calculated for all runs due to technical problems. The aerosol  
468 number concentration corresponds to the range of ~0.1 to ~3 µm and it has been calculated  
469 using the PCASP instrument. Blank entries correspond to a filter that was not collected or the  
470 instruments not working.

471



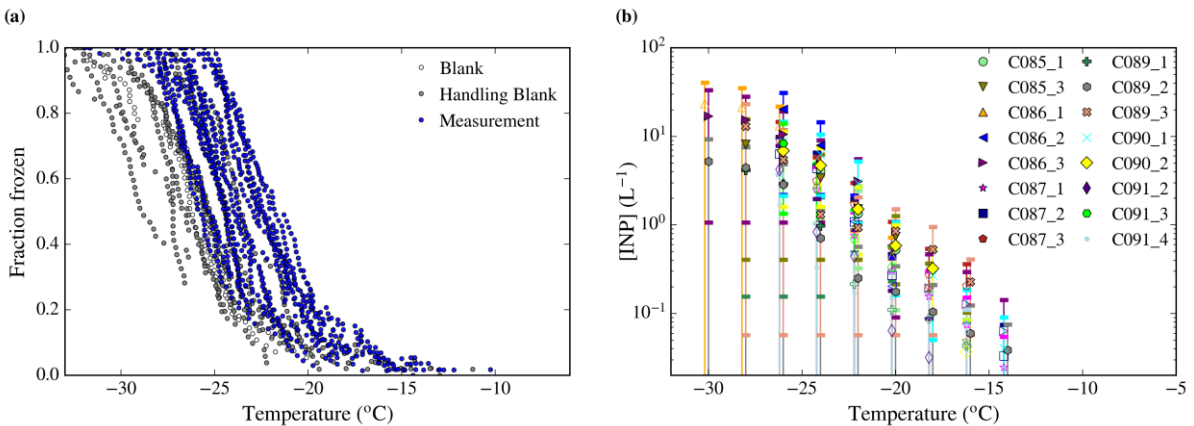


472  
 473 Figure 1. Map showing 5 day HYSPLIT back trajectories (upper panel) and altitude profile of each  
 474 back trajectory (lower panel) from the midpoint of each sample location. The sampling location is  
 475 marked using a star. The sea ice corresponds to 16<sup>th</sup> March 2018, extracted from the Multisensor  
 476 Analyzed Sea Ice Extent – Northern Hemisphere (MASIE NH) product at 1 km resolution (U.S.  
 477 National Ice Center and National Snow and Ice Data Center. Compiled by F. Fetterer, 2010). The snow  
 478 cover corresponds to the average snow cover % for March 2018, extracted from ECMWF ERA5 Land  
 479 monthly average reanalysis data (Muñoz Sabater, 2021).



480

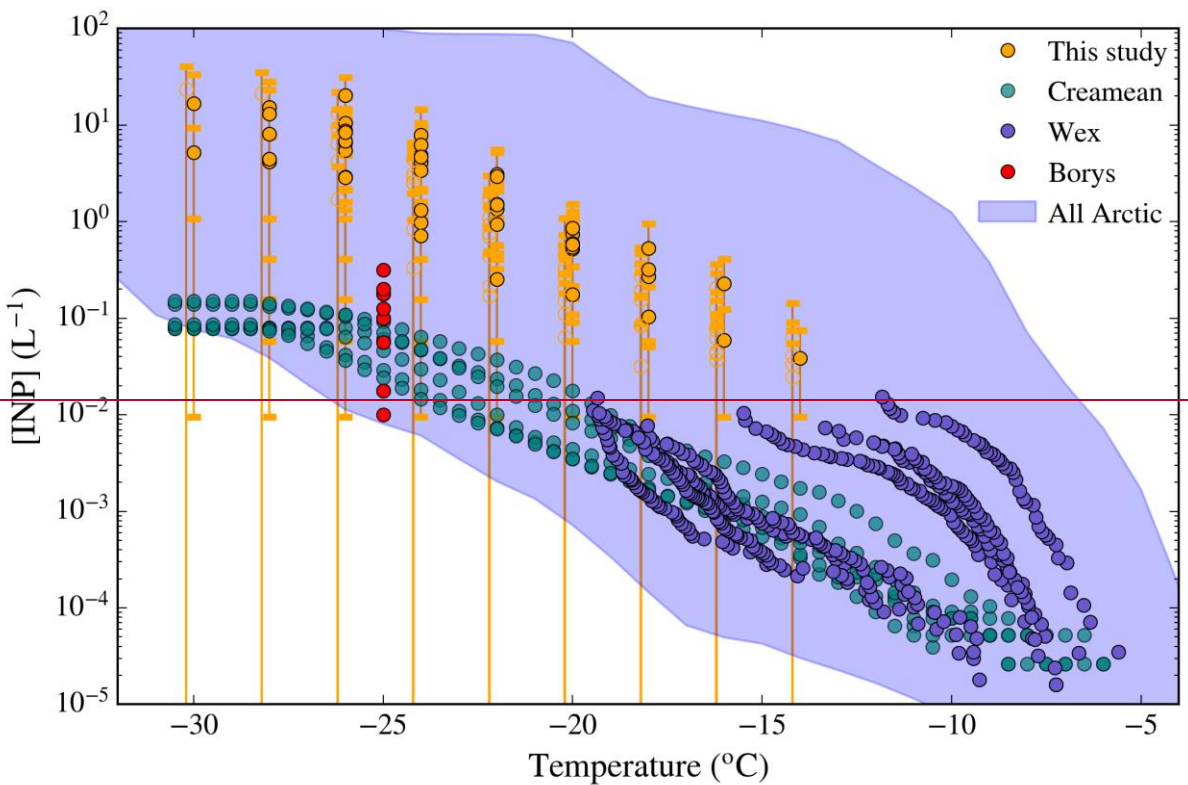
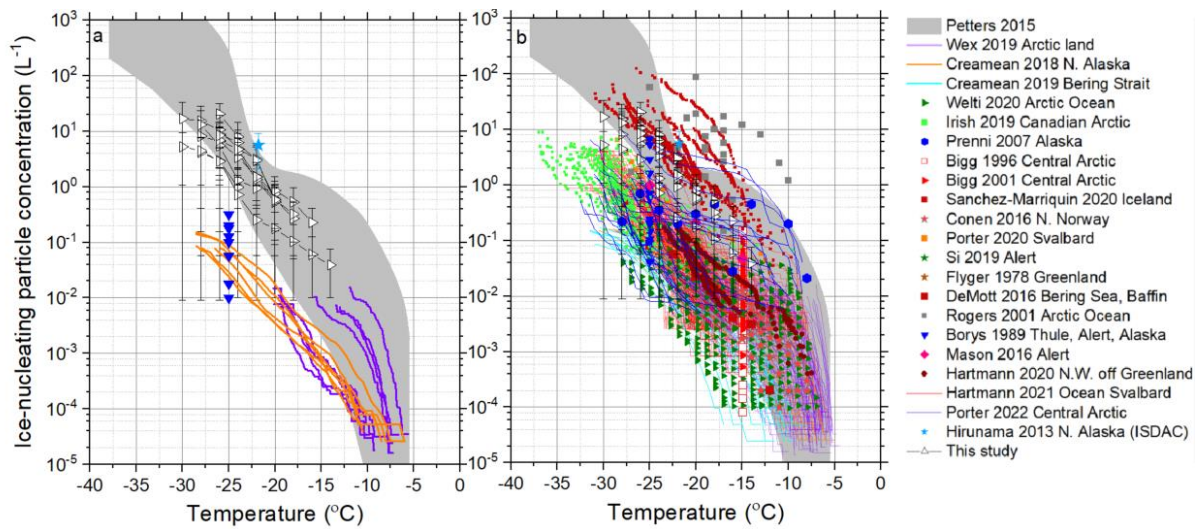
481 Figure 1. Flight tracks of the samples collected in this study and described in Table 1 (top panel). GPS  
 482 altitude at which the samples were collected (lower panel). The altitude is presented against the GTM  
 483 time at which the samples were collected (although they were collected across several days).



484

485 Figure 2. (a) Fraction of droplets frozen for all filter samples as well as blanks and handling blanks. (b)  
 486 INP particle concentrations for each filter sample. INP concentrations, upper limits and uncertainties  
 487 were calculated based on 68% confidence intervals, as shown in Appendix . Data points corresponding  
 488 to the upper limits (open symbols) have been shifted 0.2 °C along the x-axis for clarity. The way in  
 489 which the INP concentrations, upper limits and its uncertainties have been calculated are shown in  
 490 Appendix A. The criteria to determine if a measurement is above the limit of detection is based on 68%  
 491 confidence intervals.

492



496 Figure 3. INP concentrations from the present study compared with literature data. We only show our  
 497 data that was above the background (limiting values are included in Figure 2). Note that this data is  
 498 above the limit of detection based on 68% confidence intervals. The left panel is limited to a comparison  
 499 with previous measurements at nearby locations at a similar time of year (February, March and April)  
 500 (Borys, 1989;Creamean et al., 2018;Wex et al., 2019;Hiranuma et al., 2013). We also limit this  
 501 comparison to data recorded at or above water saturation, which limits the data from Hiranuma et al.  
 502 (2013) to a single point during what they describe as a relatively high INP concentration event. Note  
 503 that for the dataset of Wex et al. (2019), the concentrations increased through this period with the two  
 504 highest INP spectra from April. The right hand figure is a comparison with Arctic data in general, from  
 505 any time of the year and any location (Flyger and Heidam, 1978;Borys, 1989;Bigg, 1996;Rogers et al.,  
 506 2001;Bigg and Leck, 2001;Prenni et al., 2007;Hiranuma et al., 2013;Conen et al., 2016;DeMott et al.,

507 2016;Mason et al., 2016;Creamean et al., 2018;Wex et al., 2019;Creamean et al., 2019;Irish et al.,  
 508 2019;Si et al., 2019;Porter et al., 2020;Sanchez-Marroquin et al., 2020;Welti et al., 2020;Hartmann et  
 509 al., 2020;Hartmann et al., 2021;Porter et al., 2022). The mid-latitude data range given by Petters and  
 510 Wright (2015) is also shown.

511

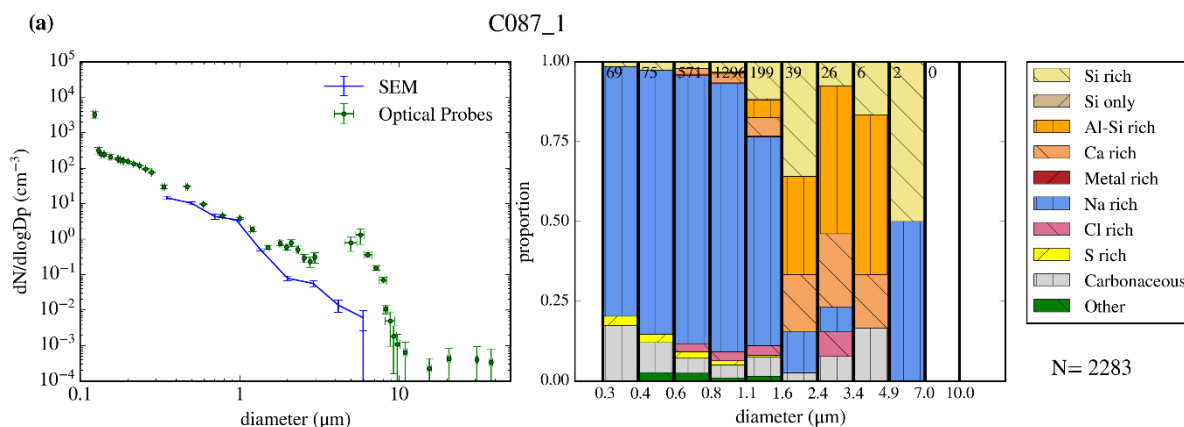
512

513 The data range corresponds to the range of all the existing INP Arctic measurements at any time of the  
 514 year in the literature, as given by Porter et al. (2022). Note that for the dataset of Wex et al. (2019), the  
 515 concentrations increased through this period with the two highest INP spectra from April. Also note  
 516 that although the upper end of the literature Arctic measurement range from Porter et al. (2022)  
 517 corresponds to the highest concentrations ever recorded in the Arctic, the majority of the Arctic  
 518 concentrations fall in the lower half of the range. The points consistent with the background (hollow  
 519 symbols) is shown with slight offsets in temperature for greater clarity of the error bars. The way in  
 520 which the INP concentrations, upper limits and its uncertainties have been calculated are shown in  
 521 Appendix , based on 68% confidence intervals.

522

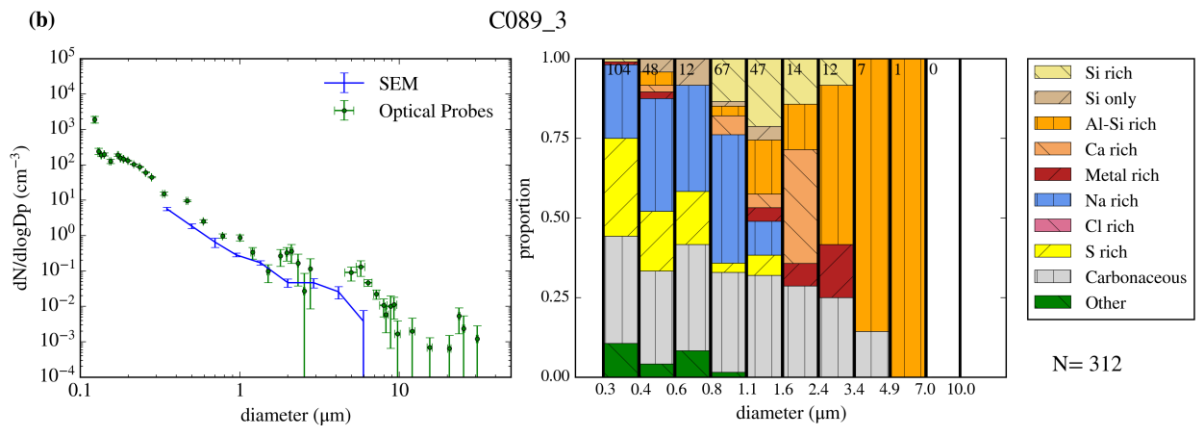
523

524

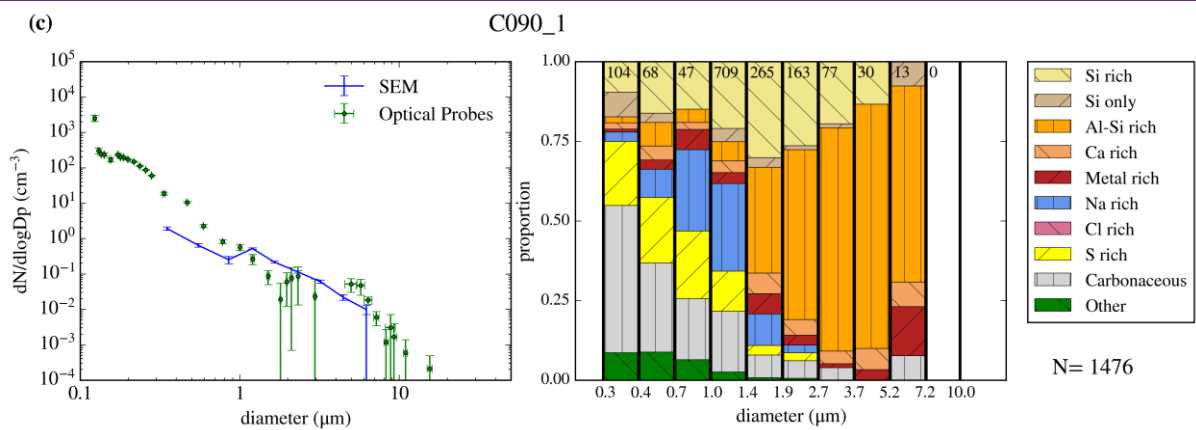


525

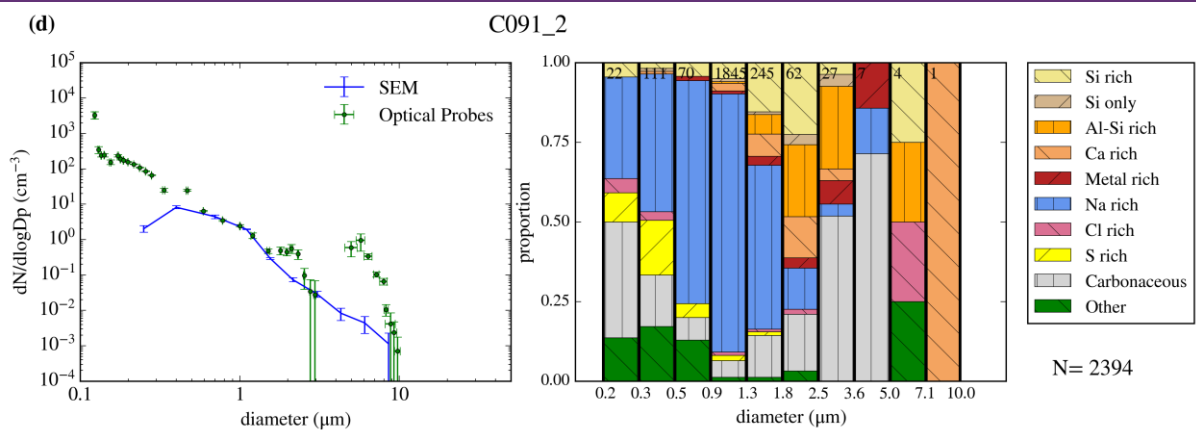




526



527



528

529 Figure 4. Results of SEM-EDS analysis of each analysed sample (a-d) showing comparison between  
 530 SEM-EDS and PCASP-CDP number size distribution (left) alongside number size-resolved  
 531 composition fractions (right).

532

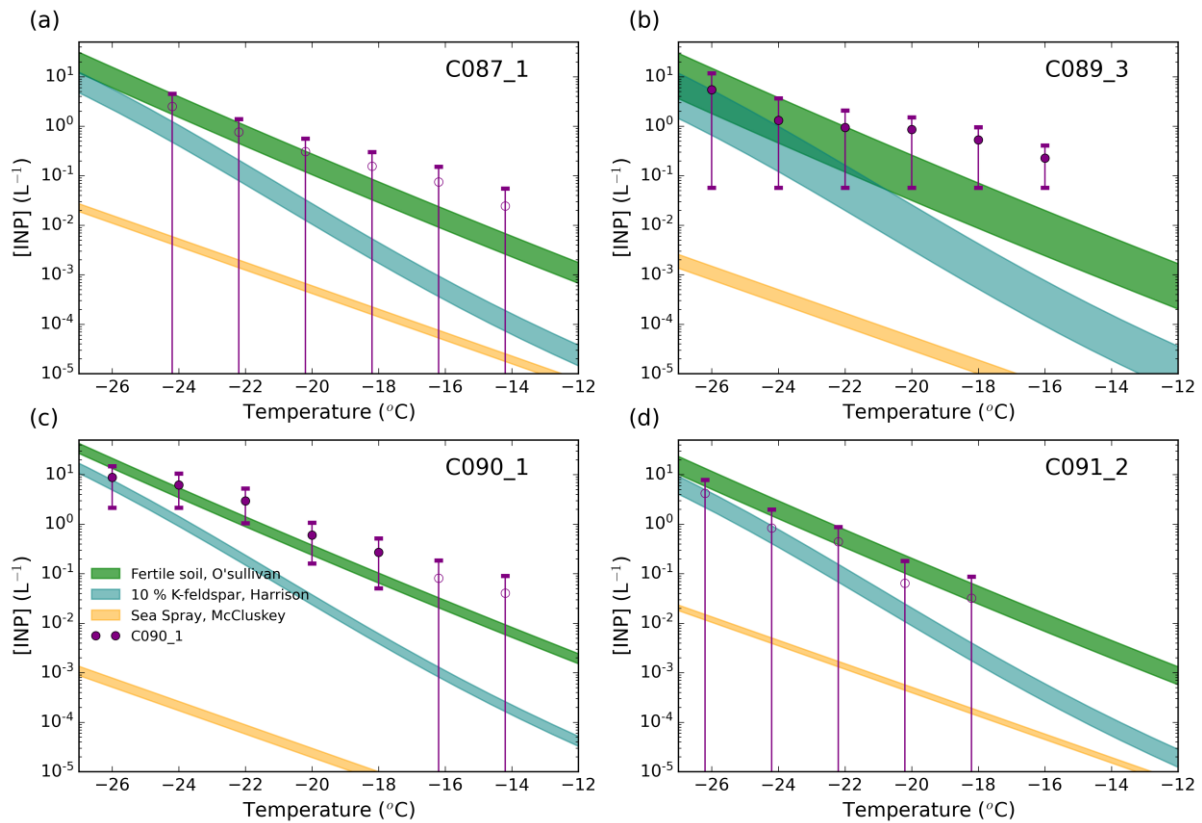
Sample	Dust area (μm <sup>2</sup> /cm <sup>3</sup> )	Dust limit of detection (μm <sup>2</sup> /cm <sup>3</sup> )	Dust <u>area</u> percentage	Sea spray aerosol area (μm <sup>2</sup> /cm <sup>3</sup> )	Sea spray <u>area</u> percentage
C087_1	<u>0.75</u>	<u>0.042</u>	<u>13.9</u>	<u>3.97</u>	<u>73.4</u>
C089_3	<u>0.57</u>	<u>0.15</u>	<u>38.1</u>	<u>0.26</u>	<u>17.1</u>
C090_1	<u>1.21</u>	<u>0.083</u>	<u>65.5</u>	<u>0.16</u>	<u>8.9</u>
C091_2	<u>0.53</u>	<u>0.051</u>	<u>11.3</u>	<u>2.79</u>	<u>59.5</u>

533

534 Table 2. Surface area of dust and sea spray aerosol from SEM-EDS analysis. The dust limit of detection  
 535 corresponds to the upper limit of the dust concentration detected on the handling blank filter based on  
 536 one standard deviation. Note that the given dust and sea spray aerosol percentages refer to surface area  
 537 percentages. The limit of detection of sea spray aerosol particles has not been indicated because the  
 538 presence of this type of particles in the handling blank is negligible. Further information on the size-  
 539 resolved composition of the handling blanks and a discussion about it can be found in (Sanchez-  
 540 Marroquin et al., 2019).

541

542



543

544 Figure 5. Predicted INP concentration of the SEM-EDS samples compared with the INP measurements  
 545 at  $-20^{\circ}C$ . The dust INP prediction has been calculated by applying different ice-nucleation  
 546 parametrizations to the surface area of dust calculated from the SEM-EDS analysis. The O'Sullivan et  
 547 al. (2014) for fertile soils and a dust containing 10 % of K-Feldspar (Harrison et al., 2019) have been  
 548 used. The NaCl INP prediction has been obtained by applying the sea spray aerosol parametrization  
 549 from McCluskey et al. (2018) to the SEM-EDS sea spray aerosol surface area. The purple points  
 550 correspond to our INP measurements or upper limits, based on 68% confidence intervals (Appendix A).

551 **Appendix A: Upper limit determination and background subtraction of the ice-nucleation**  
 552 **experiments**

553 As shown in Fig. 2a, most of the fraction of droplets frozen produced by the collected samples were  
 554 comparable or only slightly above to the ones produced by the handling blanks. Hence, we established  
 555 criteria to separate data points of the INP spectrum that are not significantly above the limit of detection  
 556 of the instrument. The analysis is performed using the differential spectrum of ice-nucleus rather than  
 557 the cumulative spectrum, which is normally used to display and compare ice-nucleation data such as  
 558 INP concentrations and densities of active sites (Vali, 1971;Vali, 2019). First, we create a histogram  
 559 with the number of freezing events per temperature interval per sample. This is done for all the samples  
 560 and handling blanks, with temperature intervals of 2 °C. We transform the number of freezing events  
 561 per interval of each sample into the differential INP spectrum,  $k(T)$ , using Eq. 1 (Vali, 2019).

$$k(T) = -\frac{1}{V\Delta T} \ln\left(1 - \frac{\Delta N}{N(T)}\right) \quad \text{Eq. 1}$$

562 In Eq. 1,  $V$  is the droplet volume,  $\Delta T$  is the temperature interval,  $\Delta N$  is the number of frozen droplets  
 563 between  $T$  and  $(T-\Delta T)$ , and  $N(T)$  is the number of unfrozen droplets at  $T$ . The  $k(T)$  values of the handling  
 564 blanks is shown in Fig B1, alongside the mean value of each interval and its standard deviation. Note  
 565 that many of the temperature intervals had zero freezing events, corresponding to  $k$  equal to zero. These  
 566 zero values cannot be seen in Fig. B1 but they have been included in the means and standard deviations.  
 567 The mean and standard deviation of the  $k$  values produced by each handling blank has been compared  
 568 with the  $k$  values corresponding to each sample. The uncertainty in the  $k$  values associated with each  
 569 sample has been calculated using a very similar Monte Carlo simulation as used previously (Vali, 2019)  
 570 using a 68 % interval. The  $k$  values associated to each sample were individually compared with the  
 571 mean and standard deviation of the  $k$  values of the handling blanks. A data point was considered above  
 572 the limit of detection when its lower error yields above the mean plus standard deviation of the blanks.  
 573 Background subtraction was applied to data points significantly above the limit of detection. This was  
 574 done by subtracting the mean of the  $k$  values of the handling blanks. The error of the background-  
 575 subtracted point was calculated by square rooting the quadratic sum of the error of the  $k_{\text{sample}}$  and  
 576  $k_{\text{background}}$ . Two examples of the comparisons between samples and the handling blanks are shown in  
 577 Fig. B2. (a) corresponds to a case where no data point was higher than the limit of detection, while (b)  
 578 corresponds to a case where most of the data points were significantly above the limit of detection. Note  
 579 that all the data measured on the 16<sup>th</sup> of March (flight C087) has been flagged as an upper limit. This is  
 580 because the handling blank experiment carried out on that day was unusually high, being compatible  
 581 with all the measurements.

582 The background corrected  $k(T)$  was integrated into the cumulative spectrum of active sites,  $K(T)$ , using  
 583 Eq. 2 (Vali, 1971;Vali, 2019).

$$K(T) = \sum_{T=0}^T k(T) \Delta T \quad \text{Eq. 2}$$

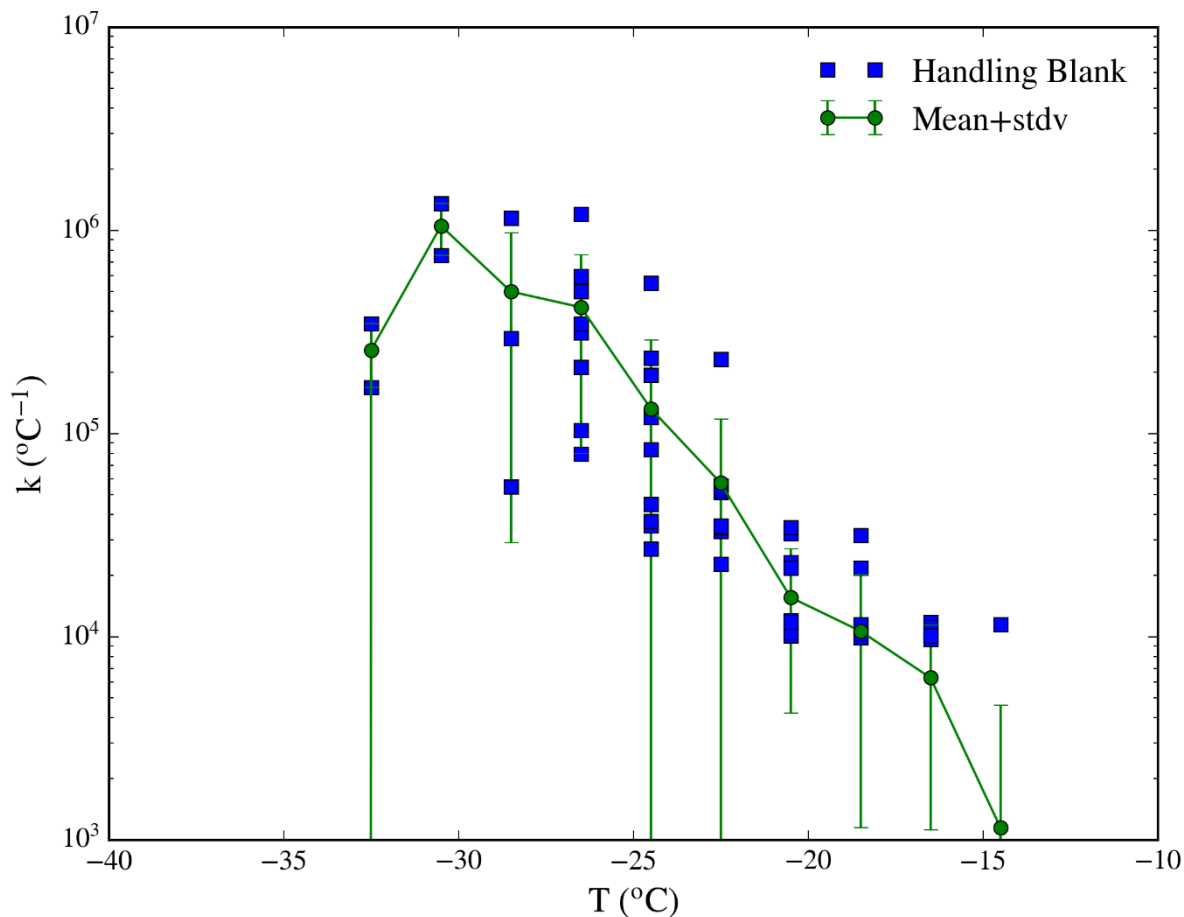
584 INP concentrations were calculated from ,  $K(T)$  using Eq. 3, where  $V_d$  is the droplet volume,  $A_{\text{filt}}$  is the  
 585 area of the filter,  $V_a$  is the sampled air volume and  $\alpha$  is the contact surface of the droplets. For this study,  
 586 we used the same values than Sanchez-Marroquin et al. (2021).

$$INP(T) = \frac{K(T)V_D A_{\text{fil}}}{V_a \alpha} \quad \text{Eq. 3}$$

587 A  $k$  value which was not significantly above the limit of detection has been represented with lower bars  
 588 going to zero in the INP spectrum (meaning upper limit to the INP concentration). However, if a  $k$  value

589 not significantly above the limit of detection was preceded by a value which was above the limit of  
590 detection, then as a result of the cumulative nature of the reported INP concentration the corresponding  
591 value is reported with a filled symbol, but the lower bound of the error bar does not change since it is  
592 possible that no new INP were present in that temperature interval. In Fig B3 one can see the INP  
593 concentration of all the samples collected in this study per each day.

594

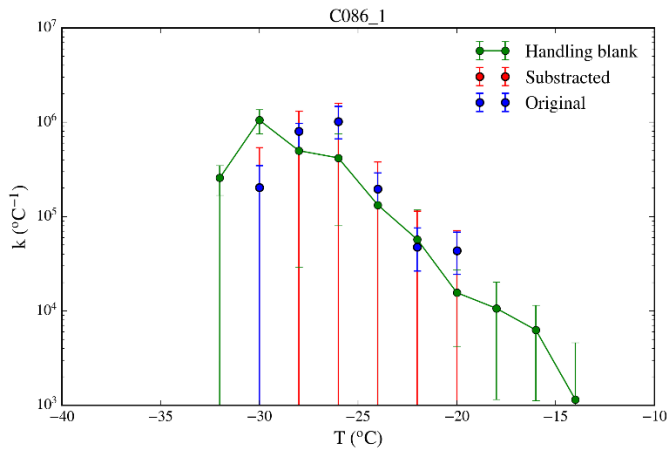


595

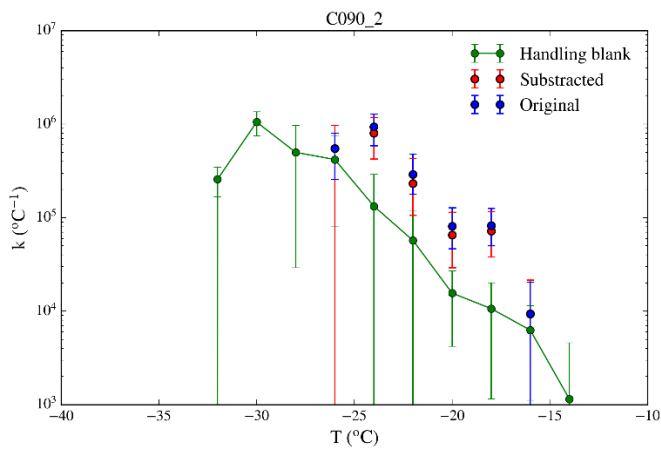
596 Figure B1. Differential spectrum of ice-nucleus of all the handling blanks performed during this  
597 campaign. Data is shown in blue, while the mean and standard deviation of the data of each bin  
598 show in green.

599



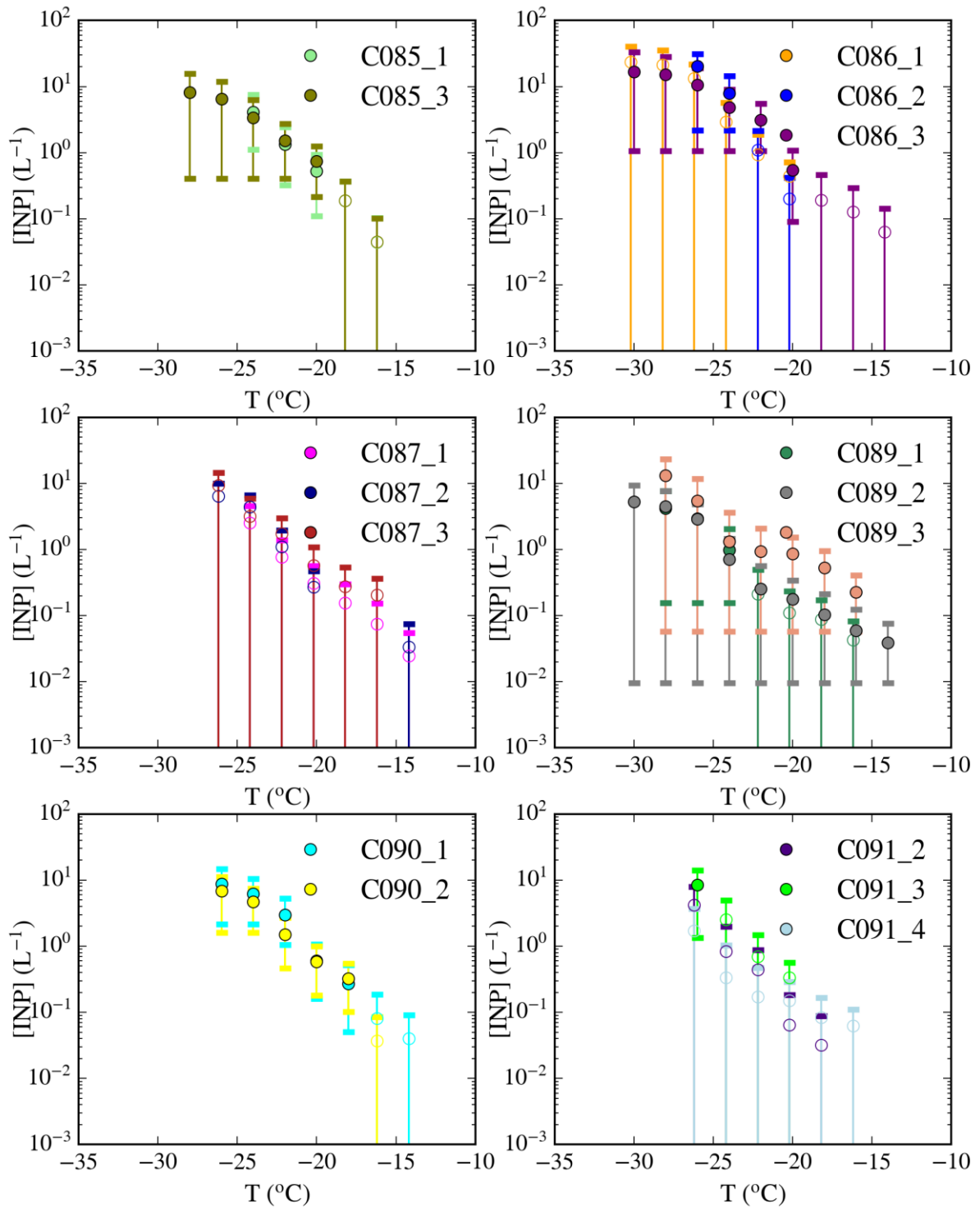


600



601

602 Figure B2. Examples of a comparison between the handling blank mean with two samples. None of the  
 603 data points of sample C086\_1 is significantly above the background. However, most of the data points  
 604 associated with sample C090\_2 are more than one error bar above the data produced by the handling  
 605 blanks and they have been background-subtracted.



606  
 607  
 608  
 609  
 610  
 611

Fig B3. INP concentrations and upper limits shown in Fig. 2 separated per sampling day. A list of the days when these samples were collected is shown in Table 1. Note that full markers corresponds to measurements above the limit of detection, while hollow markers correspond to upper limits. This has not been specified in the legend as some samples have both upper limits and measurements at the same time.

621 **References**

622  
623  
624  
625

626 Bigg, E. K.: Ice forming nuclei in the high Arctic, *Tellus B*, 48, 223-233, 10.1034/j.1600-0889.1996.t01-  
627 1-00007.x, 1996.

628 Bigg, E. K., and Leck, C.: Cloud-active particles over the central Arctic Ocean, *J. Geophys. Res. Atmos.*,  
629 106, 32155-32166, 10.1029/1999jd901152, 2001.

630 Boose, Y., Sierau, B., García, M. I., Rodríguez, S., Alastuey, A., Linke, C., Schnaiter, M., Kupiszewski, P.,  
631 Kanji, Z. A., and Lohmann, U.: Ice nucleating particles in the Saharan Air Layer, *Atmos. Chem. Phys.*,  
632 16, 9067-9087, 10.5194/acp-16-9067-2016, 2016.

633 Borys, R. D.: Studies of ice nucleation by Arctic aerosol on AGASP-II, *J. Atmos. Chem.*, 9, 169-185,  
634 10.1007/bf00052831, 1989.

635 Boucher, O., D. Randall, P. Artaxo, C. Bretherton, G. Feingold, P. Forster, V.-M. Kerminen, Y. Kondo,  
636 H. Liao, U. Lohmann, P. Rasch, S.K. Satheesh, S. Sherwood, B. Stevens and X.Y. Zhang, 2013: Climate  
637 Change 2013: The Physical Science Basis. Contribution of Working Group I to the Fifth Assessment  
638 Report of the Intergovernmental Panel on Climate Change, in, edited by: [Stocker, T. F., D. Qin, G.-K.  
639 Plattner, M. Tignor, S.K. Allen, J. Boschung, A. Nauels, Y. Xia, V. Bex and P.M. Midgley (eds.)],  
640 Cambridge University Press, Cambridge, United Kingdom and New York, NY, USA, 2013.

641 Bullard, J. E., Baddock, M., Bradwell, T., Crusius, J., Darlington, E., Gaiero, D., Gassó, S., Gisladottir,  
642 G., Hodgkins, R., McCulloch, R., McKenna-Neuman, C., Mockford, T., Stewart, H., and Thorsteinsson,  
643 T.: High-latitude dust in the Earth system, *Rev Geophys*, 54, 447-485, 10.1002/2016rg000518, 2016.

644 Carslaw, K. S.: Chapter 5 - Aerosol processes, in: *Aerosols and Climate*, edited by: Carslaw, K. S.,  
645 Elsevier, 135-185, 2022.

646 Ceppi, P., Brient, F., Zelinka, M. D., and Hartmann, D. L.: Cloud feedback mechanisms and their  
647 representation in global climate models, *Wiley Interdisciplinary Reviews: Climate Change*, 8, e465,  
648 10.1002/wcc.465, 2017.

649 Chen, Q., Mirrielees, J. A., Thanekar, S., Loeb, N. A., Kirpes, R. M., Upchurch, L. M., Barget, A. J., Lata,  
650 N. N., Raso, A. R. W., McNamara, S. M., China, S., Quinn, P. K., Ault, A. P., Kennedy, A., Shepson, P. B.,  
651 Fuentes, J. D., and Pratt, K. A.: Atmospheric particle abundance and sea salt aerosol observations in  
652 the springtime Arctic: a focus on blowing snow and leads, *Atmos. Chem. Phys.*, 22, 15263-15285,  
653 10.5194/acp-22-15263-2022, 2022.

654 Conen, F., Stopelli, E., and Zimmermann, L.: Clues that decaying leaves enrich Arctic air with ice  
655 nucleating particles, *Atmos. Environ.*, 129, 91-94, 10.1016/j.atmosenv.2016.01.027, 2016.

656 Creamean, J. M., Kirpes, R. M., Pratt, K. A., Spada, N. J., Maahn, M., de Boer, G., Schnell, R. C., and  
657 China, S.: Marine and terrestrial influences on ice nucleating particles during continuous springtime  
658 measurements in an Arctic oilfield location, *Atmos. Chem. Phys.*, 18, 18023-18042, 10.5194/acp-18-  
659 18023-2018, 2018.

660 Creamean, J. M., Cross, J. N., Pickart, R., McRaven, L., Lin, P., Pacini, A., Hanlon, R., Schmale, D. G.,  
661 Ceniceros, J., Aydell, T., Colombi, N., Bolger, E., and DeMott, P. J.: Ice Nucleating Particles Carried  
662 From Below a Phytoplankton Bloom to the Arctic Atmosphere, *Geophys Res Lett*, 46, 8572-8581,  
663 10.1029/2019gl083039, 2019.

664 Creamean, J. M., Hill, T. C. J., DeMott, P. J., Uetake, J., Kreidenweis, S., and Douglas, T. A.: Thawing  
665 permafrost: an overlooked source of seeds for Arctic cloud formation, *Environmental Research*  
666 *Letters*, 15, 10.1088/1748-9326/ab87d3, 2020.

667 Creamean, J. M., Barry, K., Hill, T. C. J., Hume, C., DeMott, P. J., Shupe, M. D., Dahlke, S., Willmes, S.,  
668 Schmale, J., Beck, I., Hoppe, C. J. M., Fong, A., Chamberlain, E., Bowman, J., Scharien, R., and  
669 Persson, O.: Annual cycle observations of aerosols capable of ice formation in central Arctic clouds,  
670 *Nat Commun*, 13, 3537, 10.1038/s41467-022-31182-x, 2022.

671 Daily, M. I., Tarn, M. D., Whale, T. F., and Murray, B. J.: An evaluation of the heat test for the ice-  
672 nucleating ability of minerals and biological material, *Atmos. Meas. Tech.*, 15, 2635-2665,  
673 10.5194/amt-15-2635-2022, 2022.

674 DeMott, P. J., Hill, T. C., McCluskey, C. S., Prather, K. A., Collins, D. B., Sullivan, R. C., Ruppel, M. J.,  
675 Mason, R. H., Irish, V. E., Lee, T., Hwang, C. Y., Rhee, T. S., Snider, J. R., McMeeking, G. R., Dhaniyala,  
676 S., Lewis, E. R., Wentzell, J. J., Abbatt, J., Lee, C., Sultana, C. M., Ault, A. P., Axson, J. L., Diaz Martinez,  
677 M., Venero, I., Santos-Figueroa, G., Stokes, M. D., Deane, G. B., Mayol-Bracero, O. L., Grassian, V. H.,  
678 Bertram, T. H., Bertram, A. K., Moffett, B. F., and Franc, G. D.: Sea spray aerosol as a unique source of  
679 ice nucleating particles, *Proc Natl Acad Sci U S A*, 113, 5797-5803, 10.1073/pnas.1514034112, 2016.  
680 Fan, S.-M.: Modeling of observed mineral dust aerosols in the arctic and the impact on winter season  
681 low-level clouds, *J. Geophys. Res. Atmos.*, 118, 11,161-111,174, 10.1002/jgrd.50842, 2013.  
682 Flyger, H., and Heidam, N. Z.: Ground level measurements of the summer tropospheric aerosol in  
683 Northern Greenland, *J. Aerosol Sci*, 9, 157-168, 10.1016/0021-8502(78)90075-7, 1978.  
684 Francis, D., Eayrs, C., Chaboureaud, J. P., Mote, T., and Holland, D. M.: Polar Jet Associated Circulation  
685 Triggered a Saharan Cyclone and Derived the Poleward Transport of the African Dust Generated by  
686 the Cyclone, *J. Geophys. Res. Atmos.*, 123, 11,899-811,917, 10.1029/2018jd029095, 2018.  
687 Frey, M. M., Norris, S. J., Brooks, I. M., Anderson, P. S., Nishimura, K., Yang, X., Jones, A. E.,  
688 Nerentorp Mastromonaco, M. G., Jones, D. H., and Wolff, E. W.: First direct observation of sea salt  
689 aerosol production from blowing snow above sea ice, *Atmos. Chem. Phys*, 20, 2549-2578,  
690 10.5194/acp-20-2549-2020, 2020.  
691 Gong, X., Wex, H., van Pinxteren, M., Triesch, N., Fomba, K. W., Lubitz, J., Stolle, C., Robinson, T. B.,  
692 Müller, T., Herrmann, H., and Stratmann, F.: Characterization of aerosol particles at Cabo Verde close  
693 to sea level and at the cloud level – Part 2: Ice-nucleating particles in air, cloud and seawater, *Atmos.*  
694 *Chem. Phys*, 20, 1451-1468, 10.5194/acp-20-1451-2020, 2020.  
695 Groot Zwaafink, C. D., Grythe, H., Skov, H., and Stohl, A.: Substantial contribution of northern high-  
696 latitude sources to mineral dust in the Arctic, *J. Geophys. Res. Atmos.*, 121, 13,678-613,697,  
697 10.1002/2016jd025482, 2016.  
698 Gunsch, M. J., Kirpes, R. M., Kolesar, K. R., Barrett, T. E., China, S., Sheesley, R. J., Laskin, A.,  
699 Wiedensohler, A., Tuch, T., and Pratt, K. A.: Contributions of transported Prudhoe Bay oil field  
700 emissions to the aerosol population in Utqiagvik, Alaska, *Atmos. Chem. Phys*, 17, 10879-10892,  
701 10.5194/acp-17-10879-2017, 2017.  
702 Harrison, A. D., Lever, K., Sanchez-Marroquin, A., Holden, M. A., Whale, T. F., Tarn, M. D., McQuaid,  
703 J. B., and Murray, B. J.: The ice-nucleating ability of quartz immersed in water and its atmospheric  
704 importance compared to K-feldspar, *Atmospheric Chemistry and Physics Discussions*, 2019, 1-23,  
705 10.5194/acp-2019-288, 2019.  
706 Harrison, A. D., O'Sullivan, D., Adams, M. P., Porter, G. C. E., Blades, E., Brathwaite, C., Chewitt-Lucas,  
707 R., Gaston, C., Hawker, R., Krüger, O. O., Neve, L., Pöhlker, M. L., Pöhlker, C., Pöschl, U., Sanchez-  
708 Marroquin, A., Sealy, A., Sealy, P., Tarn, M. D., Whitehall, S., McQuaid, J. B., Carslaw, K. S., Prospero,  
709 J. M., and Murray, B. J.: The ice-nucleating activity of African mineral dust in the Caribbean boundary  
710 layer, *Atmos. Chem. Phys. Discuss.*, 2022, 1-34, 10.5194/acp-2022-57, 2022.  
711 Hartmann, M., Adachi, K., Eppers, O., Haas, C., Herber, A., Holzinger, R., Hünerbein, A., Jäkel, E.,  
712 Jentzsch, C., Pinxteren, M., Wex, H., Willmes, S., and Stratmann, F.: Wintertime Airborne  
713 Measurements of Ice Nucleating Particles in the High Arctic: A Hint to a Marine, Biogenic Source for  
714 Ice Nucleating Particles, *Geophys Res Lett*, 47, 10.1029/2020gl087770, 2020.  
715 Hartmann, M., Gong, X., Kecorius, S., van Pinxteren, M., Vogl, T., Welti, A., Wex, H., Zeppenfeld, S.,  
716 Herrmann, H., Wiedensohler, A., and Stratmann, F.: Terrestrial or marine – indications towards the  
717 origin of ice-nucleating particles during melt season in the European Arctic up to 83.7° N, *Atmos.*  
718 *Chem. Phys*, 21, 11613-11636, 10.5194/acp-21-11613-2021, 2021.  
719 Hawker, R. E., Miltenberger, A. K., Wilkinson, J. M., Hill, A. A., Shipway, B. J., Cui, Z., Cotton, R. J.,  
720 Carslaw, K. S., Field, P. R., and Murray, B. J.: The temperature dependence of ice-nucleating particle  
721 concentrations affects the radiative properties of tropical convective cloud systems, *Atmos. Chem.*  
722 *Phys*, 21, 5439-5461, 10.5194/acp-21-5439-2021, 2021.  
723 Hiranuma, N., Brooks, S. D., Moffet, R. C., Glen, A., Laskin, A., Gilles, M. K., Liu, P., Macdonald, A. M.,  
724 Strapp, J. W., and McFarquhar, G. M.: Chemical characterization of individual particles and residuals

725 of cloud droplets and ice crystals collected on board research aircraft in the ISDAC 2008 study, *J.*  
726 *Geophys. Res. Atmos.*, **118**, 6564-6579, 10.1002/jgrd.50484, 2013.

727 Hoose, C., and Mohler, O.: Heterogeneous ice nucleation on atmospheric aerosols: a review of  
728 results from laboratory experiments, *Atmos. Chem. Phys.*, **12**, 9817-9854, 10.5194/acp-12-9817-  
729 2012, 2012.

730 Huang, J., and Jaeglé, L.: Wintertime enhancements of sea salt aerosol in polar regions consistent  
731 with a sea ice source from blowing snow, *Atmos. Chem. Phys.*, **17**, 3699-3712, 10.5194/acp-17-3699-  
732 2017, 2017.

733 Huang, Z., Huang, J., Hayasaka, T., Wang, S., Zhou, T., and Jin, H.: Short-cut transport path for Asian  
734 dust directly to the Arctic: a case study, *Environmental Research Letters*, **10**, 114018, 10.1088/1748-  
735 9326/10/11/114018, 2015.

736 Huneus, N., Schulz, M., Balkanski, Y., Griesfeller, J., Prospero, J., Kinne, S., Bauer, S., Boucher, O.,  
737 Chin, M., Dentener, F., Diehl, T., Easter, R., Fillmore, D., Ghan, S., Ginoux, P., Grini, A., Horowitz, L.,  
738 Koch, D., Krol, M. C., Landing, W., Liu, X., Mahowald, N., Miller, R., Morcrette, J. J., Myhre, G.,  
739 Penner, J., Perlwitz, J., Stier, P., Takemura, T., and Zender, C. S.: Global dust model intercomparison  
740 in AeroCom phase I, *Atmos. Chem. Phys.*, **11**, 7781-7816, 10.5194/acp-11-7781-2011, 2011.

741 Irish, V. E., Elizondo, P., Chen, J., Chou, C., Charette, J., Lizotte, M., Ladino, L. A., Wilson, T. W.,  
742 Gosselin, M., Murray, B. J., Polishchuk, E., Abbatt, J. P. D., Miller, L. A., and Bertram, A. K.: Ice-  
743 nucleating particles in Canadian Arctic sea-surface microlayer and bulk seawater, *Atmos. Chem.*  
744 *Phys.*, **17**, 10583-10595, 10.5194/acp-17-10583-2017, 2017.

745 Irish, V. E., Hanna, S. J., Willis, M. D., China, S., Thomas, J. L., Wentzell, J. J. B., Cirisan, A., Si, M.,  
746 Leaitch, W. R., Murphy, J. G., Abbatt, J. P. D., Laskin, A., Girard, E., and Bertram, A. K.: Ice nucleating  
747 particles in the marine boundary layer in the Canadian Arctic during summer 2014, *Atmos. Chem.*  
748 *Phys.*, **19**, 1027-1039, 10.5194/acp-19-1027-2019, 2019.

749 Kanji, Z. A., Ladino, L. A., Wex, H., Boose, Y., Burkert-Kohn, M., Cziczo, D. J., and Krämer, M.:  
750 Overview of Ice Nucleating Particles, *Meteorological Monographs*, **58**, 1.1-1.33,  
751 10.1175/amsmonographs-d-16-0006.1, 2017.

752 Kirpes, R. M., Bondy, A. L., Bonanno, D., Moffet, R. C., Wang, B., Laskin, A., Ault, A. P., and Pratt, K.  
753 A.: Secondary sulfate is internally mixed with sea spray aerosol and organic aerosol in the winter  
754 Arctic, *Atmos. Chem. Phys.*, **18**, 3937-3949, 10.5194/acp-18-3937-2018, 2018.

755 Kirpes, R. M., Bonanno, D., May, N. W., Fraund, M., Barget, A. J., Moffet, R. C., Ault, A. P., and Pratt,  
756 K. A.: Wintertime Arctic Sea Spray Aerosol Composition Controlled by Sea Ice Lead Microbiology, *ACS*  
757 *Cent Sci*, **5**, 1760-1767, 10.1021/acscentsci.9b00541, 2019.

758 Kirpes, R. M., Rodriguez, B., Kim, S., China, S., Laskin, A., Park, K., Jung, J., Ault, A. P., and Pratt, K. A.:  
759 Emerging investigator series: influence of marine emissions and atmospheric processing on  
760 individual particle composition of summertime Arctic aerosol over the Bering Strait and Chukchi Sea,  
761 *Environ Sci Process Impacts*, **22**, 1201-1213, 10.1039/c9em00495e, 2020.

762 Komurcu, M., Storelvmo, T., Tan, I., Lohmann, U., Yun, Y., Penner, J. E., Wang, Y., Liu, X., and  
763 Takemura, T.: Intercomparison of the cloud water phase among global climate models, *J. Geophys.*  
764 *Res. Atmos.*, **119**, 3372-3400, 10.1002/2013jd021119, 2014.

765 Korolev, A., McFarquhar, G., Field, P. R., Franklin, C., Lawson, P., Wang, Z., Williams, E., Abel, S. J.,  
766 Axisa, D., Borrmann, S., Crosier, J., Fugal, J., Krämer, M., Lohmann, U., Schlenker, O., Schnaiter, M.,  
767 and Wendisch, M.: Mixed-Phase Clouds: Progress and Challenges, *Meteorological Monographs*, **58**,  
768 5.1-5.50, 10.1175/amsmonographs-d-17-0001.1, 2017.

769 Lewis, E., and Schwartz, S.: Sea Salt Aerosol Production: Mechanisms, Methods, Measurements and  
770 Models—A Critical Review, *GMS*, **152**, 3719, 10.1029/GM152, 2004.

771 Lindsley, W. G.: Filter Pore Size and Aerosol Sample Collection, *NIOSH Manual of Analytical Methods*,  
772 1-14, 2016.

773 Mason, R. H., Si, M., Chou, C., Irish, V. E., Dickie, R., Elizondo, P., Wong, R., Brintnell, M., Elsasser, M.,  
774 Lassar, W. M., Pierce, K. M., Leaitch, W. R., MacDonald, A. M., Platt, A., Toom-Sauntry, D., Sarda-  
775 Esteve, R., Schiller, C. L., Suski, K. J., Hill, T. C. J., Abbatt, J. P. D., Huffman, J. A., DeMott, P. J., and



776 Bertram, A. K.: Size-resolved measurements of ice-nucleating particles at six locations in North  
777 America and one in Europe, *Atmos. Chem. Phys.*, 16, 1637-1651, 10.5194/acp-16-1637-2016, 2016.  
778 May, N. W., Quinn, P. K., McNamara, S. M., and Pratt, K. A.: Multiyear study of the dependence of  
779 sea salt aerosol on wind speed and sea ice conditions in the coastal Arctic, *J. Geophys. Res. Atmos.*,  
780 121, 9208-9219, 10.1002/2016jd025273, 2016.

781 McCluskey, C. S., Ovadnevaite, J., Rinaldi, M., Atkinson, J. D., Belosi, F., Ceburnis, D., Marullo, S., Hill,  
782 T. C. J., Lohmann, U., Kanji, Z. A., O'Dowd, C., Kreidenweis, S. M., and DeMott, P. J.: Marine and  
783 Terrestrial Organic Ice-Nucleating Particles in Pristine Marine to Continentally Influenced Northeast  
784 Atlantic Air Masses, *J. Geophys. Res. Atmos.*, 123, 6196-6212, 10.1029/2017jd028033, 2018.

785 McCoy, D. T., Tan, I., Hartmann, D. L., Zelinka, M. D., and Storelvmo, T.: On the relationships among  
786 cloud cover, mixed-phase partitioning, and planetary albedo in GCMs, *Journal of Advances in*  
787 *Modeling Earth Systems*, 8, 650-668, 10.1002/2015ms000589, 2016.

788 McCoy, D. T., Hartmann, D. L., and Zelinka, M. D.: Chapter 9 - Mixed-Phase Cloud Feedbacks, in:  
789 *Mixed-Phase Clouds*, edited by: Andronache, C., Elsevier, 215-236, 2018.

790 Meinander, O., Dagsson-Waldhauserova, P., Amosov, P., Aseyeva, E., Atkins, C., Baklanov, A., Baldo,  
791 C., Barr, S., Barzycka, B., Benning, L., Cvetkovic, B., Enchilik, P., Frolov, D., Gassó, S., Kandler, K.,  
792 Kasimov, N., Kavan, J., King, J., Koroleva, T., Krupskaya, V., Kusiak, M., Laska, M., Lasne, J.,  
793 Lewandowski, M., Luks, B., McQuaid, J., Moroni, B., Murray, B., Möhler, O., Nawrot, A., Nickovic, S.,  
794 O'Neill, N., Pejanovic, G., Popovicheva, O., Ranjbar, K., Romanias, M., Samonova, O., Sanchez-  
795 Marroquin, A., Schepanski, K., Semenkov, I., Sharapova, A., Shevnina, E., Shi, Z., Sofiev, M., Thevenet,  
796 F., Thorsteinsson, T., Timofeev, M., Umo, N. S., Uppstu, A., Urupina, D., Varga, G., Werner, T.,  
797 Arnalds, O., and Vukovic Vimic, A.: Newly identified climatically and environmentally significant high  
798 latitude dust sources, *Atmos. Chem. Phys. Discuss.*, 2021, 1-74, 10.5194/acp-2021-963, 2021.

799 Ménégoz, M., Voltaire, A., Teyssédre, H., Méliá, D. S. y., Peuch, V. H., and Gouttevin, I.: How does  
800 the atmospheric variability drive the aerosol residence time in  
801 the Arctic region?, *Tellus B: Chemical and Physical Meteorology*, 64, 10.3402/tellusb.v64i0.11596,  
802 2012.

803 Muñoz Sabater, J.: ERA5-Land monthly averaged data from 1981 to present, in, edited by: (CDS), C.  
804 C. C. S. C. S. C. D. S., 2021.

805 Murray, B. J., O'Sullivan, D., Atkinson, J. D., and Webb, M. E.: Ice nucleation by particles immersed in  
806 supercooled cloud droplets, *Chem Soc Rev*, 41, 6519-6554, 10.1039/c2cs35200a, 2012.

807 Murray, B. J., Carslaw, K. S., and Field, P. R.: Opinion: Cloud-phase climate feedback and the  
808 importance of ice-nucleating particles, *Atmos. Chem. Phys.*, 21, 665-679, 10.5194/acp-21-665-2021,  
809 2021.

810 O'Sullivan, D., Murray, B. J., Malkin, T. L., Whale, T. F., Umo, N. S., Atkinson, J. D., Price, H. C.,  
811 Baustian, K. J., Browse, J., and Webb, M. E.: Ice nucleation by fertile soil dusts: relative importance of  
812 mineral and biogenic components, *Atmos. Chem. Phys.*, 14, 1853-1867, 10.5194/acp-14-1853-2014,  
813 2014.

814 O'Sullivan, D., Murray, B. J., Ross, J. F., Whale, T. F., Price, H. C., Atkinson, J. D., Umo, N. S., and  
815 Webb, M. E.: The relevance of nanoscale biological fragments for ice nucleation in clouds, *Sci Rep*, 5,  
816 8082, 10.1038/srep08082, 2015.

817 Petters, M. D., and Wright, T. P.: Revisiting ice nucleation from precipitation samples, *Geophys Res*  
818 *Lett*, 42, 8758-8766, 10.1002/2015gl065733, 2015.

819 Porter, G. C. E., Sikora, S. N. F., Adams, M. P., Proske, U., Harrison, A. D., Tarn, M. D., Brooks, I. M.,  
820 and Murray, B. J.: Resolving the size of ice-nucleating particles with a balloon deployable aerosol  
821 sampler: the SHARK, *Atmos. Meas. Tech.*, 13, 2905-2921, 10.5194/amt-13-2905-2020, 2020.

822 Porter, G. C. E., Adams, M. P., Brooks, I. M., Ickes, L., Karlsson, L., Leck, C., Salter, M. E., Schmale, J.,  
823 Siegel, K., Sikora, S. N. F., Tarn, M. D., Vüllers, J., Wernli, H., Zieger, P., Zinke, J., and Murray, B. J.:  
824 Highly Active Ice-Nucleating Particles at the Summer North Pole, *J. Geophys. Res. Atmos.*, 127, 28,  
825 10.1029/2021jd036059, 2022.

826 Prenni, A. J., Harrington, J. Y., Tjernström, M., DeMott, P. J., Avramov, A., Long, C. N., Kreidenweis, S.  
827 M., Olsson, P. Q., and Verlinde, J.: Can Ice-Nucleating Aerosols Affect Arctic Seasonal Climate?,  
828 *Bulletin of the American Meteorological Society*, 88, 541-550, 10.1175/bams-88-4-541, 2007.

829 Prenni, A. J., Demott, P. J., Rogers, D. C., Kreidenweis, S. M., McFarquhar, G. M., Zhang, G., and  
830 Poellot, M. R.: Ice nuclei characteristics from M-PACE and their relation to ice formation in clouds,  
831 *Tellus B*, 61, 436-448, 10.1111/j.1600-0889.2009.00415.x, 2009.

832 Price, H. C., Baustian, K. J., McQuaid, J. B., Blyth, A., Bower, K. N., Choularton, T., Cotton, R. J., Cui, Z.,  
833 Field, P. R., Gallagher, M., Hawker, R., Merrington, A., Miltenberger, A., Neely Iii, R. R., Parker, S. T.,  
834 Rosenberg, P. D., Taylor, J. W., Trembath, J., Vergara-Temprado, J., Whale, T. F., Wilson, T. W.,  
835 Young, G., and Murray, B. J.: Atmospheric Ice-Nucleating Particles in the Dusty Tropical Atlantic, *J.*  
836 *Geophys. Res. Atmos.*, 123, 2175-2193, 10.1002/2017jd027560, 2018.

837 Reicher, N., Segev, L., and Rudich, Y.: The Welzmann Supercooled Droplets Observation on  
838 a Microarray (WISDOM) and application for ambient dust, *Atmos. Meas. Tech.*, 11, 233-248,  
839 10.5194/amt-11-233-2018, 2018.

840 Rinaldi, M., Hiranuma, N., Santachiara, G., Mazzola, M., Mansour, K., Paglione, M., Rodriguez, C. A.,  
841 Traversi, R., Becagli, S., Cappelletti, D., and Belosi, F.: Ice-nucleating particle concentration  
842 measurements from Ny-Ålesund during the Arctic spring–summer in 2018, *Atmos. Chem. Phys*, 21,  
843 14725-14748, 10.5194/acp-21-14725-2021, 2021.

844 Rogers, D. C., DeMott, P. J., and Kreidenweis, S. M.: Airborne measurements of tropospheric ice-  
845 nucleating aerosol particles in the Arctic spring, *J. Geophys. Res. Atmos.*, 106, 15053-15063,  
846 10.1029/2000jd900790, 2001.

847 Rolph, G., Stein, A., and Stunder, B.: Real-time Environmental Applications and Display sYstem:  
848 READY, *Environ. Model. Software*, 95, 210-228, 10.1016/j.envsoft.2017.06.025, 2017.

849 Rosenberg, P. D., Dean, A. R., Williams, P. I., Dorsey, J. R., Minikin, A., Pickering, M. A., and Petzold,  
850 A.: Particle sizing calibration with refractive index correction for light scattering optical particle  
851 counters and impacts upon PCASP and CDP data collected during the Fennec campaign, *Atmos.*  
852 *Meas. Tech.*, 5, 1147-1163, 10.5194/amt-5-1147-2012, 2012.

853 Ryder, C. L., Marengo, F., Brooke, J. K., Estelles, V., Cotton, R., Formenti, P., McQuaid, J. B., Price, H.  
854 C., Liu, D. T., Ausset, P., Rosenberg, P. D., Taylor, J. W., Choularton, T., Bower, K., Coe, H., Gallagher,  
855 M., Crosier, J., Lloyd, G., Highwood, E. J., and Murray, B. J.: Coarse-mode mineral dust size  
856 distributions, composition and optical properties from AER-D aircraft measurements over the  
857 tropical eastern Atlantic, *Atmos. Chem. Phys*, 18, 17225-17257, 10.5194/acp-18-17225-2018, 2018.

858 Sanchez-Marroquin, A., Hedges, D. H. P., Hiscock, M., Parker, S. T., Rosenberg, P. D., Trembath, J.,  
859 Walshaw, R., Burke, I. T., McQuaid, J. B., and Murray, B. J.: Characterisation of the filter inlet system  
860 on the FAAM BAe-146 research aircraft and its use for size-resolved aerosol composition  
861 measurements, *Atmos. Meas. Tech.*, 12, 5741-5763, 10.5194/amt-12-5741-2019, 2019.

862 Sanchez-Marroquin, A., Arnalds, O., Baustian-Dorsi, K. J., Browse, J., Dagsson-Waldhauserova, P.,  
863 Harrison, A. D., Maters, E. C., Pringle, K. J., Vergara-Temprado, J., Burke, I. T., McQuaid, J. B., Carslaw,  
864 K. S., and Murray, B. J.: Iceland is an episodic source of atmospheric ice-nucleating particles relevant  
865 for mixed-phase clouds, *Science Advances*, 6, eaba8137, 10.1126/sciadv.aba8137, 2020.

866 Sanchez-Marroquin, A., West, L. S., Burke, I. T., McQuaid, J. B., and Murray, B. J.: Mineral and  
867 biological ice-nucleating particles above the South East of the British Isles, 2021.

868 Santl-Temkiv, T., Lange, R., Beddows, D., Rauter, U., Pilgaard, S., Dall'Osto, M., Gunde-Cimerman, N.,  
869 Massling, A., and Wex, H.: Biogenic Sources of Ice Nucleating Particles at the High Arctic Site Villum  
870 Research Station, *Environ Sci Technol*, 53, 10580-10590, 10.1021/acs.est.9b00991, 2019.

871 Schnell, R. C.: Airborne ice nucleus measurements around the Hawaiian Islands, *J. Geophys. Res.*, 87,  
872 8886, 10.1029/JC087iC11p08886, 1982.

873 Shi, Y., Liu, X., Wu, M., Ke, Z., and Brown, H.: Relative Importance of High-Latitude Local and Long-  
874 Range Transported Dust to Arctic Ice Nucleating Particles and Impacts on Arctic Mixed-Phase Clouds,  
875 *Atmos. Chem. Phys. Discuss.*, 2021, 1-57, 10.5194/acp-2021-621, 2021.

876 Shi, Y., Liu, X., Wu, M., Zhao, X., Ke, Z., and Brown, H.: Relative importance of high-latitude local and  
877 long-range-transported dust for Arctic ice-nucleating particles and impacts on Arctic mixed-phase  
878 clouds, *Atmos. Chem. Phys*, 22, 2909-2935, 10.5194/acp-22-2909-2022, 2022.

879 Si, M., Evoy, E., Yun, J., Xi, Y., Hanna, S. J., Chivulescu, A., Rawlings, K., Veber, D., Platt, A., Kunkel, D.,  
880 Hoor, P., Sharma, S., Leaitch, W. R., and Bertram, A. K.: Concentrations, composition, and sources of  
881 ice-nucleating particles in the Canadian High Arctic during spring 2016, *Atmos. Chem. Phys*, 19, 3007-  
882 3024, 10.5194/acp-19-3007-2019, 2019.

883 Soo, J. C., Monaghan, K., Lee, T., Kashon, M., and Harper, M.: Air sampling filtration media:  
884 Collection efficiency for respirable size-selective sampling, *Aerosol Sci Technol*, 50, 76-87,  
885 10.1080/02786826.2015.1128525, 2016.

886 Stein, A. F., Draxler, R. R., Rolph, G. D., Stunder, B. J. B., Cohen, M. D., and Ngan, F.: NOAA's HYSPLIT  
887 Atmospheric Transport and Dispersion Modeling System, *Bulletin of the American Meteorological  
888 Society*, 96, 2059-2077, 10.1175/bams-d-14-00110.1, 2015.

889 Storelvmo, T., Tan, I., and Korolev, A. V.: Cloud Phase Changes Induced by CO<sub>2</sub> Warming—a Powerful  
890 yet Poorly Constrained Cloud-Climate Feedback, *Current Climate Change Reports*, 1, 288-296,  
891 10.1007/s40641-015-0026-2, 2015.

892 Tan, I., Storelvmo, T., and Zelinka, M. D.: Observational constraints on mixed-phase clouds imply  
893 higher climate sensitivity, *Science*, 352, 224-227, 10.1126/science.aad5300, 2016.

894 Tobo, Y., Adachi, K., DeMott, P. J., Hill, T. C. J., Hamilton, D. S., Mahowald, N. M., Nagatsuka, N.,  
895 Ohata, S., Uetake, J., Kondo, Y., and Koike, M.: Glacially sourced dust as a potentially significant  
896 source of ice nucleating particles, *Nat Geosci*, 12, 253-+, 10.1038/s41561-019-0314-x, 2019.

897 U.S. National Ice Center and National Snow and Ice Data Center. Compiled by F. Fetterer, M. S., S.  
898 Helfrich, and P. Clemente-Colón: Multisensor Analyzed Sea Ice Extent - Northern Hemisphere  
899 (MASIE-NH) in, 1 ed., Boulder, Colorado USA. National Snow and Ice Data Center, 2010.

900 Ullrich, R., Hoose, C., Mohler, O., Niemand, M., Wagner, R., Hohler, K., Hiranuma, N., Saathoff, H.,  
901 and Leisner, T.: A New Ice Nucleation Active Site Parameterization for Desert Dust and Soot, *J.  
902 Atmospheric Sci.*, 74, 699-717, 10.1175/Jas-D-16-0074.1, 2017.

903 Vali, G.: Quantitative Evaluation of Experimental Results on the Heterogeneous Freezing Nucleation  
904 of Supercooled Liquids, *J. Atmospheric Sci.*, 28, 402-409, 10.1175/1520-  
905 0469(1971)028<0402:QEOERA>2.0.CO;2, 1971.

906 Vali, G.: Revisiting the differential freezing nucleus spectra derived from drop-freezing experiments:  
907 methods of calculation, applications, and confidence limits, *Atmos. Meas. Tech.*, 12, 1219-1231,  
908 10.5194/amt-12-1219-2019, 2019.

909 VanCuren, R. A., Cahill, T., Burkhart, J., Barnes, D., Zhao, Y., Perry, K., Cliff, S., and McConnell, J.:  
910 Aerosols and their sources at Summit Greenland – First results of continuous size- and time-resolved  
911 sampling, *Atmos. Environ.*, 52, 82-97, 10.1016/j.atmosenv.2011.10.047, 2012.

912 Vergara-Temprado, J., Murray, B. J., Wilson, T. W., O'Sullivan, D., Browse, J., Pringle, K. J., Ardon-  
913 Dryer, K., Bertram, A. K., Burrows, S. M., Ceburnis, D., DeMott, P. J., Mason, R. H., O'Dowd, C. D.,  
914 Rinaldi, M., and Carslaw, K. S.: Contribution of feldspar and marine organic aerosols to global ice  
915 nucleating particle concentrations, *Atmos. Chem. Phys*, 17, 3637-3658, 10.5194/acp-17-3637-2017,  
916 2017.

917 Vergara-Temprado, J., Miltenberger, A. K., Furtado, K., Grosvenor, D. P., Shipway, B. J., Hill, A. A.,  
918 Wilkinson, J. M., Field, P. R., Murray, B. J., and Carslaw, K. S.: Strong control of Southern Ocean cloud  
919 reflectivity by ice-nucleating particles, *Proc Natl Acad Sci U S A*, 115, 2687-2692,  
920 10.1073/pnas.1721627115, 2018.

921 Welti, A., Bigg, E. K., DeMott, P. J., Gong, X., Hartmann, M., Harvey, M., Henning, S., Herenz, P., Hill,  
922 T. C. J., Hornblow, B., Leck, C., Löffler, M., McCluskey, C. S., Rauker, A. M., Schmale, J., Tatzelt, C., van  
923 Pinxteren, M., and Stratmann, F.: Ship-based measurements of ice nuclei concentrations over the  
924 Arctic, Atlantic, Pacific and Southern oceans, *Atmos. Chem. Phys*, 20, 15191-15206, 10.5194/acp-20-  
925 15191-2020, 2020.

926 Wex, H., Huang, L., Zhang, W., Hung, H., Traversi, R., Becagli, S., Sheesley, R. J., Moffett, C. E.,  
927 Barrett, T. E., Bossi, R., Skov, H., Hünnerbein, A., Lubitz, J., Löffler, M., Linke, O., Hartmann, M.,  
928 Herenz, P., and Stratmann, F.: Annual variability of ice-nucleating particle concentrations at different  
929 Arctic locations, *Atmos. Chem. Phys.*, 19, 5293-5311, 10.5194/acp-19-5293-2019, 2019.  
930 Whale, T. F., Murray, B. J., O'Sullivan, D., Wilson, T. W., Umo, N. S., Baustian, K. J., Atkinson, J. D.,  
931 Workneh, D. A., and Morris, G. J.: A technique for quantifying heterogeneous ice nucleation in  
932 microlitre supercooled water droplets, *Atmos. Meas. Tech.*, 8, 2437-2447, 10.5194/amt-8-2437-  
933 2015, 2015.  
934 Wilson, T. W., Ladino, L. A., Alpert, P. A., Breckels, M. N., Brooks, I. M., Browse, J., Burrows, S. M.,  
935 Carslaw, K. S., Huffman, J. A., Judd, C., Kilhau, W. P., Mason, R. H., McFiggans, G., Miller, L. A.,  
936 Najera, J. J., Polishchuk, E., Rae, S., Schiller, C. L., Si, M., Vergara-Temprado, J., Whale, T. F., Wong, J.  
937 P., Wurl, O., Yakobi-Hancock, J. D., Abbatt, J. P., Aller, J. Y., Bertram, A. K., Knopf, D. A., and Murray,  
938 B. J.: A marine biogenic source of atmospheric ice-nucleating particles, *Nature*, 525, 234-238,  
939 10.1038/nature14986, 2015.  
940 Yang, X., Pyle, J. A., and Cox, R. A.: Sea salt aerosol production and bromine release: Role of snow on  
941 sea ice, *Geophys Res Lett*, 35, 1-5, 10.1029/2008gl034536, 2008.  
942 Young, G., Jones, H. M., Darbyshire, E., Baustian, K. J., McQuaid, J. B., Bower, K. N., Connolly, P. J.,  
943 Gallagher, M. W., and Choularton, T. W.: Size-segregated compositional analysis of aerosol particles  
944 collected in the European Arctic during the ACCACIA campaign, *Atmos. Chem. Phys.*, 16, 4063-4079,  
945 DOI 10.5194/acp-16-4063-2016, 2016.  
946 Yun, J., Evoy, E., Worthy, S. E., Fraser, M., Veber, D., Platt, A., Rawlings, K., Sharma, S., Leaitch, W. R.,  
947 and Bertram, A.: Ice nucleating particles in the Canadian High Arctic during the fall of 2018,  
948 *Environmental Science: Atmospheres*, 10.1039/d1ea00068c, 2022.  
949 Zhao, X., Huang, K., Fu, J. S., and Abdullaev, S. F.: Long-range transport of Asian dust to the Arctic:  
950 identification of transport pathways, evolution of aerosol optical properties, and impact assessment  
951 on surface albedo changes, *Atmos. Chem. Phys.*, 22, 10389-10407, 10.5194/acp-22-10389-2022,  
952 2022.  
953  
954